DYNAMIC ANALYSIS OF INTELLIGENT LOAD FREQUENCY CONTROL OF INTERCONNECTED NONLINEAR CONVENTIONAL AND RENEWABLE POWER SYSTEM

RAJIB MONDAL

Department of Electrical and Electronic Engineering

BRAC University

Dhaka, Bangladesh.

May 2018

DYNAMIC ANALYSIS OF INTELLIGENT LOAD FREQUENCY CONTROL OF INTERCONNECTED NONLINEAR CONVENTIONAL AND RENEWABLE POWER SYSTEM

By

Rajib Mondal
ID: 12161004

Supervised by

Dr. Md. Mosaddequr Rahman

Professor, Department of Electrical and Electronic Engineering
BRAC University, Dhaka, Bangladesh.

This thesis is submitted in partial fulfillment of the requirements for the Degree of Master of Science (M. Sc.) at the Department of Electrical and Electronic Engineering,
BRAC University, Dhaka, Bangladesh.

May 2018

APPROVAL

The thesis entitled, "DYNAMIC ANALYSIS OF INTELLIGENT LOAD FREQUENCY CONTROL OF INTERCONNECTED NONLINEAR CONVENTIONAL AND RENEWABLE POWER SYSTEM" submitted by Rajib Mondal, ID no. 12161004 has been accepted as satisfactory in partial fulfillment of the requirement for the degree of Master of Science in Electrical and Electronic Engineering on 22nd May 2018.

BOARD OF EXAMINERS

1.

Dr. Shahidul Islam Khan — Chairman
Professor and Chairperson
Department of Electrical and Electronic Engineering
BRAC University
Dhaka-1212, Bangladesh.

2.

Dr. Md. MosaddequrRahman — Supervisor & Member
Professor
Department of Electrical and Electronic Engineering
BRAC University, Dhaka, Bangladesh.

3.

Dr. Amina Hasan Abedin — Member
Assistant Professor
Department of Electrical and Electronic Engineering
BRAC University, Dhaka, Bangladesh.

4.

Dr. Tareq Aziz — Member (External)
Associate Professor
Department of Electrical and Electronic Engineering
Ahsanullah University of Science and Technology
Dhaka, Bangladesh.

DECLARATION

It is hereby declared that this thesis titled "DYNAMIC ANALYSIS OF INTELLIGENT LOAD FREQUENCY CONTROL OF INTERCONNECTED NONLINEAR CONVENTIONAL AND RENEWABLE POWER SYSTEM" or any part of it has not been submitted elsewhere for the award of any other degree or diploma. A paper has been accepted and presented in the conference on 6th July 2017, International Conference on Intelligent Computing, Instrumentation and Control Technologies (ICICICT), Kerala, India, IEEE. https://ieeexplore.ieee.org/document/8342596/.

Signature of the Author

(Rajib Mondal)
ID#12161004
M. Sc. in EEE
Department of EEE
BRAC University
Bangladesh.

DEDICATION

This thesis is dedicated to my parents.

ACKNOWLEDGEMENTS

I would like to express my deepest sense of gratitude towards my supervisor, Dr. Md. Mosaddequr Rahman, Professor, Department of Electrical and Electronic Engineering, BRAC University, Dhaka, Bangladesh who has given me much suggestion, guidance and support.

I would like to thank all the honorable teachers and staff members of Department of Electrical and Electronic Engineering, BRAC University for their extended cooperation and guidance. I also take this opportunity to give thanks to others who have given me support of my study at BRAC University.

ABSTRACT

In this thesis, a variable structure concept sliding mode based load frequency control is developed on a two-area interconnected power system. The power system contains reheat, and hydraulic turbines which are distributed in these two areas respectively. Both governor dead band and generation rate constraint are included in the model of this power system. Our control goal is to regulate the frequency error, tie-line power error and area control error despite the presences of external load disturbance and system uncertainties. The sliding mode based load frequency controller is simulated on this two-area interconnected nonlinear power system. The simulation results verify the effectiveness of the controller.

The main idea behind the development is to design the performance evaluation based on fuzzy controller for two areas interconnected hydro-thermal power plant is proposed. To enhance the performance of fuzzy logic controller sliding surface is included. The sliding concept arises due to variable structure concept (VSC). The objective of VSC has been greatly extended from stabilization to other control functions. The most distinguished feature of VSC is its ability to result in very robust control systems.

In control system, sliding mode control is a nonlinear control method that alters the dynamics of a nonlinear system by application of a discontinuous control signal that forces the system to "slide" along a cross section of the systems normal behavior. It can switch from one continuous structure to another based on the current position in the state space. The multiple control structures are designed so that trajectories always move toward an adjacent region with a different control structure and so the ultimate trajectory will not exist entirely within one control structure. Instead, it will slide along the boundaries of the control structures. The motion of the system as it slides along these boundaries is called a sliding mode and the geometrical locus consisting of the boundaries is called the sliding surface. The method alters the dynamics of a nonlinear system by application of a high-frequency switching control.

The proposed sliding mode control method is compared with proportional integral and hybrid neuro fuzzy control method. Here, proportional integral and hybrid neuro fuzzy control method is chosen because it is a dominant control method in industry for the load frequency control. The time required to stay 2% to 5% of any response final value that is the settling time of this response. The designed model confirms that settling time is consider for 0.01% of final value and it shows the robustness, stability and high performance of the controller. The settling time of the designed controller is 24.66 seconds and 25.65 seconds for combined hydro-thermal plant frequency and tie line power deviation respectively. The settling time of the designed controller is minimum compare to other controllers.

A new unique model is developed using generation rate constraint and governor dead band which is applied in variable structure concept sliding mode fuzzy logic controller. The model gives better dynamics compare to conventional models. The proposed fuzzy logic controller maintains the stability and proves its superiority compared to other conventional fuzzy models. The settling time, percent of peak overshoots, frequency deviations of proposed model are much better than other conventional fuzzy controller. Simulation results demonstrate the effectiveness of the control strategy by successfully driving the frequency error and tie-line error; it shows the robustness of the controller against compare to other controller.

TABLE OF CONTENTS

LIST OF FIGURES

LIST OF TABLES

LIST OF ABBREVIATIONS

LFC	: Load Frequency Control
AGC	: Automatic Generation Control
FLC	: Fuzzy Logic Control
VSC	: Variable Structure Concept
SMC	: Sliding Mode Control
PI	: Proportional Integral
PID	: Proportional-Integral-Derivative
HNF	: Hybrid Neuro Fuzzy
GA	: Genetic Algorithm
ANN	: Artificial Neural Network
ACE	: Area Control Error
GDB	: Governor Dead Band
GRC	: Generation Rate Constraint

NOMENCLATURE

T_{12} : Synchronizing Coefficient

B_i : Frequency Bias Constant

T_{sg} : Time Constant of Steam Governor

Q : Reactive Power

f : System Frequency

P_{ari} : Area Rated Power

H_{gi} : Inertia Constant

Δp_{di} : Incremental Load Change

ΔP_{gi} : Incremental Change of Generation Power

K_{rc} : Reheat Constant

T_{rc} : Reheat Time Constant

T_{st} : Time Constant of Steam Turbine

R_i : Speed Regulation Parameter of Governor

T_{spi} : $\frac{2H_{gi}}{fD_{gi}}$, K_{pi} : $\frac{1}{D_{gi}K_j}$: Integral Gain

K_d, K_p, K_i : Electric Governor Derivative, Proportional and Integral Gains

K_t : Fuzzy Logic Control Feedback Gain

T_w : Starting Time of Water

ACE : Area Control Error

P : Rated Power

E : Source Voltage

V : Terminal Voltage

$\Delta\theta$: Voltage Angle

$\Delta\delta$: Variation of Angle

ΔP : Variation of Power

Δf : Supply Frequency Variation

V_f : Generator Field Voltage

Δp_c : Power Variation of Speed Changer Position

K_H : Gain of Speed Governor

R : Speed Regulation of the Governor

T_{HG} : Time Constant of Speed Governor

K_{pi} : $\frac{1}{B}$: Power System Gain

T_{sp} : $\frac{2H}{Bf_0}$: Time Constant of Power System

Chapter 1
INTRODUCTION

1.1 Background

In an interconnected power system that consists of several control areas, as the system varies, the tie-line power will change and the frequency deviations will occur. The load frequency control is a part of the automatic generation control (AGC) system. The objective of LFC is to damp the transient deviations in area frequency and tie line power interchange. The control error signal in LFC is called area control error (ACE), which represents the real power imbalance between generation and load. The ACE is a linear combination of net tie line power error and frequency error. This signal is used to regulate the generator output power based on network load demand. Different types of controllers have been proposed in literature for the load frequency control [1]. The proportional integral (PI) controller is the historical type of load frequency controller [2]. Since the PI controller parameters are usually tuned based on experience and classical or trial-and-error approaches, it cannot obtain good dynamic performance for a wide range of operating conditions and various load variation scenarios in a multi-area power system [5]. Large scale power systems are normally composed of control areas or regions representing coherent groups of generators. In a practically interconnected power system, the generation normally comprises of a mix of thermal, hydro, nuclear and gas power generation. However, owing to their high efficiency, nuclear plants are usually kept at base load close to their maximum output with no participation in the system automatic generation control (AGC). Gas power generation is ideal for meeting the varying load demand. Gas plants are used to meet peak demands only. Thus the natural choice for AGC falls on either thermal or hydro units. Automatic Generation Control (AGC) or Load Frequency Control (LFC) is a very important issue in power system operation and control for supplying sufficient and reliable electric power with good quality. AGC is a feedback control system adjusting a generator output power to remain defined frequency. One of the objectives of AGC is to maintain the system frequency at nominal value (50 Hz). In the steady state operation of power system, the load demand is increased or decreased in the form of kinetic energy stored in generator prime mover set, which results the variation of speed and frequency accordingly. Therefore, the control of load frequency is essential to have safe operation of the power system. The LFC issues have been tackled with by the various researchers in different time through AGC regulator, excitation controller design and control performance with respect to parameter variation/uncertainties and different load characteristics. As the configuration of the modern power system is complex, the oscillation incurred subjected to any disturbance may spread to wide areas leading

to system black out [4]. In this context, advance control methodology such as optimal control, variable structure control, adaptive control, self-tuning control, robust and intelligent control were applied in LFC problem. Now, there is rapid momentum in the progress of the research to tackle the LFC in the deregulated environment, LFC with communication delay, and LFC with new energy systems. Dynamic analysis of variable structure based sliding mode intelligent load frequency control of interconnected nonlinear conventional and renewable power system has been carried out using advanced fuzzy logic controller.

1.2 The Concept of Load Frequency Control

Load frequency control is an important control problem in the dynamical operation of interconnected power systems. The purpose of the load frequency controller is to keep the system frequency and the inter-area tie power as near as possible to the scheduled values during normal operation, and when the system is subject to disturbances or sudden changes in load demands. The input mechanical power to the generators is used to control the frequency of the output electrical power and to maintain the power exchange between the areas as scheduled. A well designed and operated power system should be able to cope with changes in the load and with system disturbances; and it should provide acceptably high level of power quality while maintaining both voltage and frequency within tolerable limits. The fundamental objectives of load frequency control are: (1) to maintain the system frequency at the nominal value, (2) to hold the interchange power among areas at scheduled value, and (3) to share the amount of required generation among generating units in a preset manner [5].

1.3 The Problems

In order to design load frequency controllers to achieve high power quality standards, there is a need for data transmission over long distances. The transmission of such data is costly, and it induces errors; the probability of system disturbances is high. Such problem has been tackled by either (1) using fuzzy logic controller sliding surface stabilization without consideration of the performance of the overall system from an economical point of view, or (2) considering the system as if it is completely decentralized and designed local controllers which ignore the inter-actions between the multi-areas of the system [5].

1.4 Literature Review

The load frequency control problem has been investigated by many researchers. Khodabakh et al. [5] obtained an optimum integral and proportional integral (PI) controller by using the concept of stability and techniques with conventional area control error (ACE). W. Tan and Z. Xu [6] proposed a decentralized (PI) biased dual mode controllers for two area interconnected thermal power system. Some researchers developed a generalized approach based on the concepts of discontinuous control, dual-mode control and variable structure systems. The proposed generalized approach was used to develop an LFC algorithm which was tested on a multi-area interconnected power system. Ghoshal et al. [7] devised a proportional, integral and derivative control scheme based on the feedback of averaged derivatives to realize a noise-tolerable differential control with its application to the LFC in power systems and proposed an adaptive controller for the LFC problem of power systems where the controller uses a PI adaptation. Rerkpreedapong et al. [8] examined the use of a two-level control scheme for a two-area power system with nonlinear interactions between the areas and proposed a multilevel adaptive load frequency controller which is based on the self tuning regulator using Robust load frequency controlusing genetic algorithms and linear matrix inequalities. Hassan et al. [10] developed a flexible automatic generation control (AGC) algorithm for the LFC problem. Also proposed a simple, robust controller, which is based on the Riccati equation approach; only the bounds of the system parameters are required to design an Automatic Generation Control of Interconnected Power System by Hybrid Neuro Fuzzy Approach. In addition, several researchers have used intelligent control to deal with the LFC problem. Golpira et al. [15] proposed a robust load frequency controller using genetic algorithms and linear matrix inequalities for Indirect Adaptive Fuzzy Logic frequency control of Multi-area Power System applied a robust control technique to a nonlinear LFC problem. Yousef et al.[11] used an artificial neural network controller for the LFC problem. Hosseini et al. [13] Hybrid Neuro Fuzzy (HNF) approach is employed for an Automatic Generation Control (AGC) of interconnected power system with and without generation rate constraint (GRC). Other works on the application of intelligent control techniques to the load frequency control problem were reported in the literature see [14, 17].

In this thesis, the rules for the gains are chosen to be identical in order to improve the system performance. The comparison of the proposed fuzzy logic controller and the conventional PI controllers suggests that the overshoots and settling time with the proposed FLC controller are better than the rest. In this paper, the main idea behind the development is to design the performance evaluation based on Fuzzy controller for two areas interconnected hydro-thermal power plant is proposed. To enhance the performance of fuzzy logic controller sliding surface is included. The sliding concept arises due to variable structure concept (VSC). The objective of VSC has been greatly extended from stabilization to

other control functions. In control system, sliding mode control, or SMC, is a nonlinear control method that alters the dynamics of a nonlinear system by application of a discontinuous control signal that forces the system to "slide" along a cross-section of the system's normal behavior. The state-feedback control law is not a continuous function of time. Instead, it can switch from one continuous structure to another based on the current position in the state space. Hence, sliding mode control is a variable structure control method. The multiple control structures are designed so that trajectories always move toward an adjacent region with a different control structure, and so the ultimate trajectory will not exist entirely within one control structure. Instead, it will slide along the boundaries of the control structures. The motion of the system as it slides along these boundaries is called a sliding mode[29] and the geometrical locus consisting of the boundaries is called the sliding (hyper)surface. In the context of modern control theory, any variable structure system, like a system under SMC, may be viewed as a special case of a hybrid dynamical system as the system both flows through a continuous state space but also moves through different discrete control modes. Variable structure control (VSC) is a form of discontinuous nonlinear control. The method alters the dynamics of a nonlinear system by application of a high-frequency switching control [30].The main mode of VSC operation is dynamic sliding mode control (SMC). The strengths of SMC include:

- Low sensitivity to plant parameter uncertainty
- Greatly reduced-order modeling of plant dynamics
- Finite-time convergence (due to discontinuous control law)

The control objectives are as follows

- Each control area as for as possible should supply its own load demand and power transfer through tie line should be on mutual agreement.
- Both control areas should controllable to the frequency control.

1.5 Scopes of the Research

In this dissertation, we develop a decentralized, continuous, variable structure dynamic sliding-mode-based load frequency control (LFC) on a two-area interconnected power system with external load disturbance and system uncertainties. Reheat turbine and hydraulic turbine are distributed in two different areas respectively. The nonlinearities such as the governor dead band (GDB) and generation rate constraint (GRC) are included in the block diagram model of the power system. It is the first time for a SMC to be applied to a continuous, interconnected power system with two different kinds of turbines

(including reheat turbine and hydraulic turbines) for load frequency control. The sliding mode based LFC is tested on the power system with both load disturbance and parameter variations. It is also the first time that a continuous sliding mode based LFC is applied to such an interconnected uncertain power system with load disturbance. The FSMC is simulated on a two-area interconnected nonlinear power system in Matlab/Simulink. Simulation results demonstrate the effectiveness of the control strategy by successfully driving the frequency error and tie-line error; it shows the robustness of the controller against compare to other controller.

1.6 Thesis Organization

The dissertation is organized as follows. In Chapter II, we introduce with the basic fuzzy logic controller, fuzzy inference rule, membership function, proportional integral controller and hybrid nuro fuzzy controller.

In Chapter III, the composition of a two-area interconnected nonlinear power system and develop the mathematical model based on the power system. In Chapter IV, a variable structure concept sliding mode based load frequency controller is developed on this interconnected power system model. In Chapter V, the fuzzy sliding mode based LFC is simulated on single area and two-area interconnected power system with governor's dead band and generation rate constraint. Simulation results are presented and show the robustness of the controller compare with other controller. In Chapter V, we make concluding remarks and suggest future research directions.

Chapter 2
FUZZY LOGIC CONTROLLER

2.1 Fuzzy Logic Control

Fuzzy logic is an intelligent process or problem-solving control methodology incorporated in control system engineering, to control systems when inputs are either imprecise or the mathematical models are not present at all. Fuzzy logic can process a reasonable number of inputs but the system complexity increases with the increase in the number of inputs and outputs, therefore distributed processors would probably be easier to implement. fuzzification is process of making a crisp quantity into the fuzzy. They carry considerable uncertainty. If the form of uncertainty occurs to arise because of imprecision, ambiguity, or vagueness, then the variable is probably fuzzy and can be represented by a membership function. defuzzification is the conversion of a fuzzy quantity to a crisp quantity, just as fuzzification is the conversion of a precise quantity to a fuzzy quantity. The output of a fuzzy process can be the logical union of two or more fuzzy membership functions defined on the universe of discourse of the output variables. There are many methods of defuzzification, variable structure concept (VSC) operation of sliding mode control (SMC) which smallest of maximum method is applied in creating fuzzy inference system. SOM (Smallest of Maximum) Method: This is also called first (or last of maximum) and this method uses the overall output or union of all individual output fuzzy sets C_k to determine the smallest value of the domain with maximum z membership degree in C_k. The equation for Z^* are as follows

$$Z^* = \inf_{z \in Z} \{ z \in Z \mid \mu C_K(Z) = hgt(C_K) \} \qquad (2.1)$$

The Fuzzy logic control includes of three main stages, namely the fuzzification interface, the inference rules engine and the defuzzification interface. For Load Frequency Control the process operator is assumed to respond to variables area control error (*e*) and change of area control error (*Ce*).

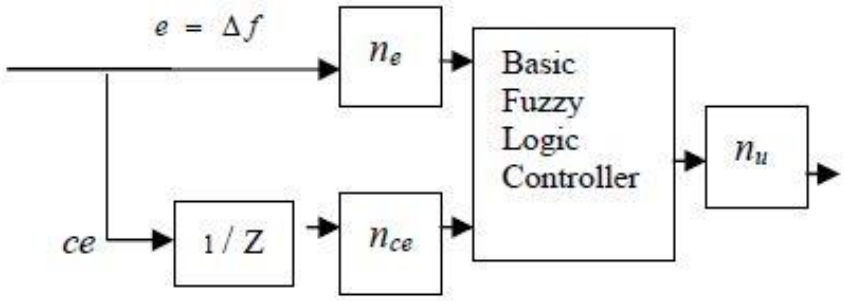

Figure 2.1 Block diagram of a Fuzzy Logic controller

The variable error is equal to the real power system frequency deviation (Δf). The frequency deviation Δf, is the difference between the nominal or scheduled power system frequency (f_N) and the real power system frequency (f). Taking the scaling gains into account, the global function of the FLC output signal can be written as

$$\Delta Pc = F [n_c \, e(k), n_{ce} \, Ce(k)] \qquad (2.2)$$

Where n_c and n_{ce} are the error and the change of error scaling gains, respectively, and F is a fuzzy nonlinear function. FLC is dependent to its inputs scaling gains. The block diagram of FLC is shown in Fig 4. nu is output control gain . A label set corresponding to linguistic variables of the input control signals, e(k) and Ce(k), with a sampling time of 0.01sec is as follows

$$L(e, Ce) = \{ NB, NM, ZE, PM, PB\}, \qquad (2.3)$$

Where, NB = Negative Big, NM = Negative Medium,

ZE = Zero, PM = Positive Medium, PB = Positive Big.

There are three principal elements to a fuzzy logic controller

1. Fuzzification module (Fuzzifier)
2. Inference rule engine
3. Defuzzification module (Defuzzifier)

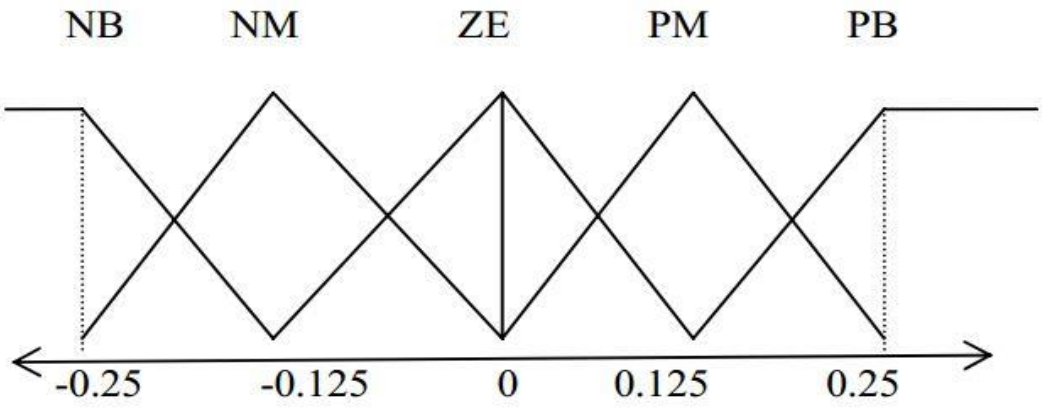

Figure 2.2 Membership function for the control input variables

Table 2.1 Fuzzy Inference Rule for Fuzzy Logic Control

Input	*e(k)*					
		NB	NM	ZE	PM	PB
ce(k)	NB	NB	NB	NM	NM	ZE
	NM	NB	NB	NM	ZE	ZE
	ZE	NM	NM	ZE	PM	PM
	PM	ZE	PM	PM	PB	PB
	PB	ZE	ZE	PM	PB	PB

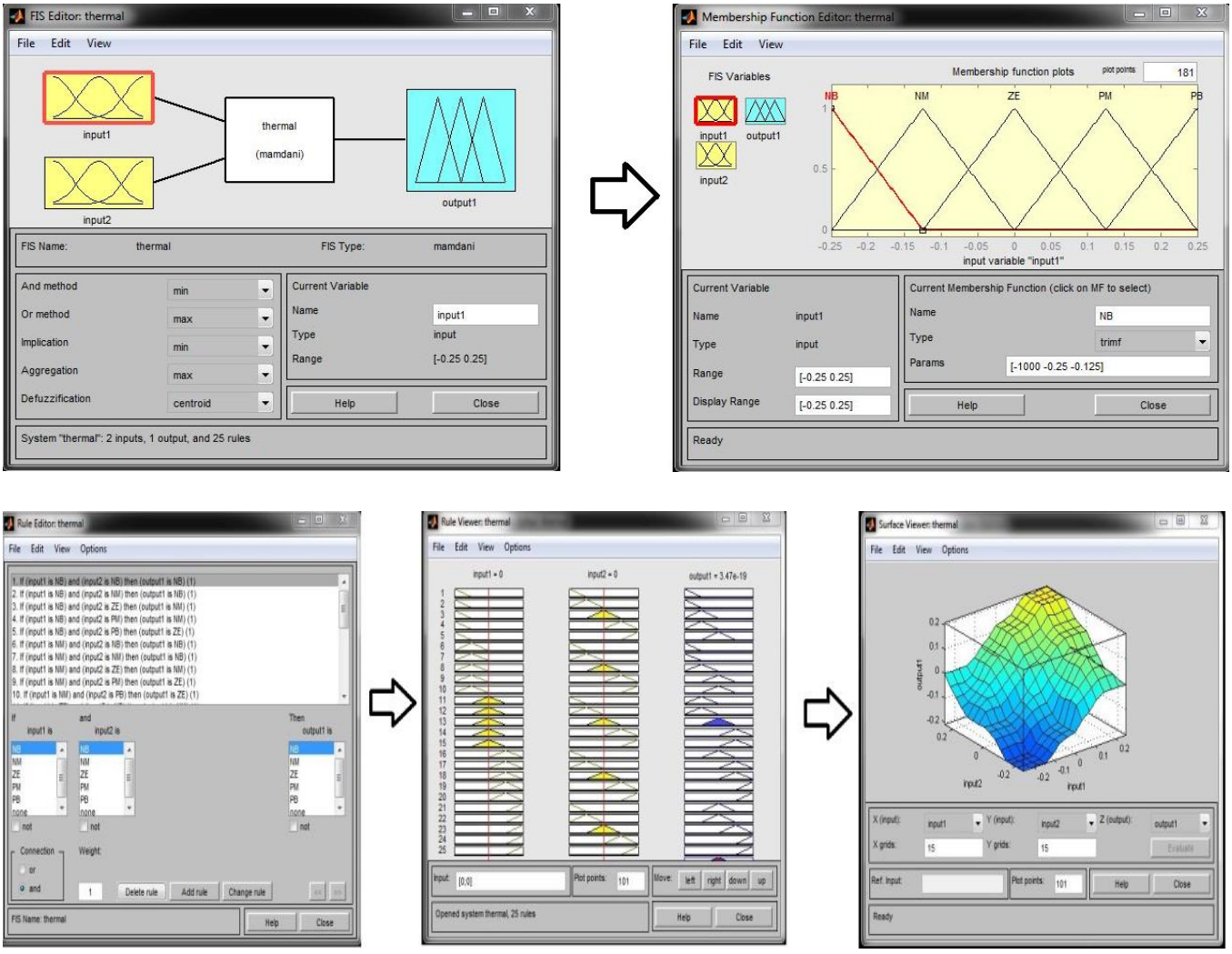

Figure 2.3 Setting up of membership function rules in MATLAB SIMULINK

For Load Frequency Control the process operator is assumed to respond variables error (e) and change of error (Ce) (that is frequency deviation and change in frequency deviation). Attempt has been made to examine with five number of triangular membership functions (MFs) which gives better dynamic response with the range on input (error in frequency deviation and change in frequency deviation) i.e universe of discourse is -0.25 to 0.25. The numbers of rules are 25. The membership functions (MFs) for the input variables are shown in Figure 1.3 and Setting up of membership function rules in MATLAB shown in Figure 1.4. Table 1.1 shows the rules. The rules are interpreted as if ACE e(k) is NB an d/dt(ACE) Ce(k) is ZE then the output is NM. Triangular membership functions are used for both the inputs and output.

2.2 Conventional Integral Controller

Conventional proportional plus integral controller (PI) offers zero steady state frequency deviation, but it exhibits poor dynamic performance (such as more number of oscillation and more settling time), especially in the presence of parameters variation and nonlinearity [4]. In PI Controller Proportionality constant provides simplicity, reliability, directness etc. The disadvantage of offset in it is eliminated by integration but this system will have some oscillatory offset. The task of load frequency controller is to generate a control signal u_i that keeps system frequency and tie-line interchange power at predetermined values [4].

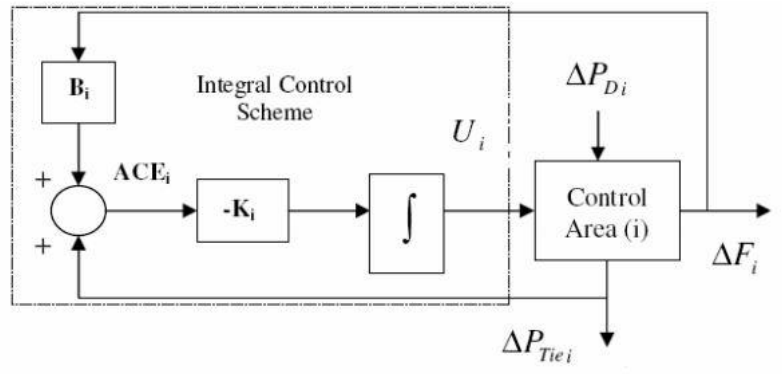

Figure 2.4: Conventional PI controller

$$u_i = -Ki\int_0^{\tau}(ACEi)dt = -Ki\int_0^{\tau}(\Delta Ptie,i + bi\Delta fi)dt \tag{2.4}$$

When an integral controller is added to each area of the uncontrolled plant in forward path the steady state error in the frequency becomes zero. The task of load frequency controller is to generate a control signal u that maintains system frequency and tie-line interchange power at predetermined values [2]. The block diagram of PI controller is shown in figure 2.4. Conventional Proportional plus Integral controller (PI) provides zero steady state frequency deviation, but it exhibits poor dynamic performance (such as number of oscillation and more settling time), especially in the presence of parameters variation and nonlinearity [5].

2.3 Hybrid Neuro Fuzzy (HNF)

A neuro-fuzzy system is a fuzzy system that uses a learning algorithm derived from neural network theory to determine its parameters (fuzzy sets and fuzzy rules) by processing data samples. In recent years, hybrid neuro-fuzzy (HNF) approach [13] has considerable attention for their useful applications in the fields like control, pattern recognition, image processing, etc. In all these applications there are different neuro-fuzzy applications designed for different purposes and fields. Hybrid neuro-fuzzy results are found from fusion of neural network and fuzzy logic. According to real world requirements, the linguistic variables have to be transformed to crisp output. Centre of gravity method is the best well-known defuzzification method and used in this research work. Sugeno type of defuzzification method is adopted in this HNF approach. It obtains the center of area occupied by the fuzzy set. It is given by the expression

$$X = \frac{\int \mu(x)x dx}{\int \mu(x) dx} \qquad (2.5)$$

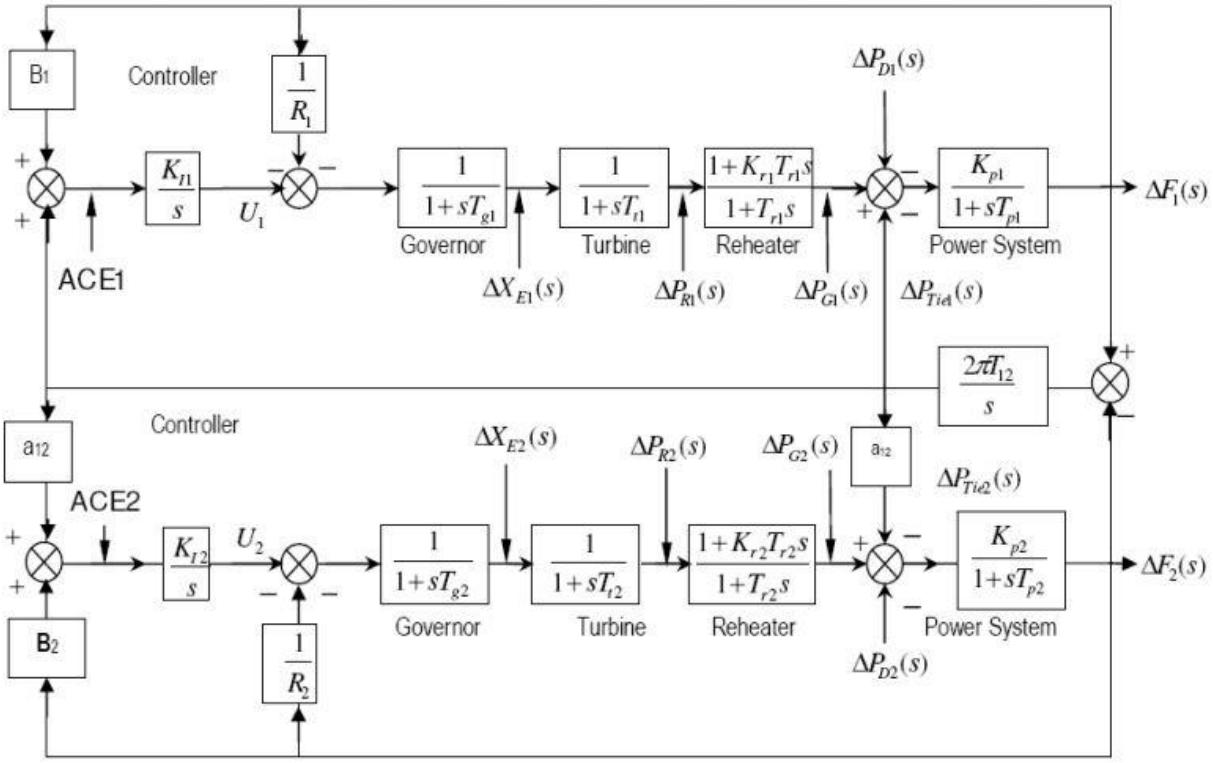

Fig. 2.5 Transfer function model of two-area power system

Steps to design HNF Controller

1. Draw the Simulink model with FLC and simulate it with the given rule base.

2. The first step to design the HNF controller is collecting the training data while simulating with FLC.

3. The two inputs i.e. ACE and d(ACE)/dt and the output signal gives the training data.

4. Use a fis edit to create the HNF.fis file.

5. Load the training data collected in Step.1 and generates the FIS with MF's.

6. Train the collected data with generated FIS up to a particular no. of epochs.

The HNF utilizes sugeno-type fuzzy inference system controller, with the parameters inside the fuzzy inference system decided by the neural-network back propagation method [13]. The ANFIS is designed by taking ACE and rate of change of ACE as inputs. There are different memberships functions associated with each input and output response. In this design, the trapezoidal membership function is used for input and output variables. The number of membership function determines the quality of control which can be achieved using fuzzy controller. As the number of membership function increases, the quality of control improves. As the number of linguistic variables increases, the computational time and required memory increases. Therefore, a compromise between the quality of control and computational time is needed to choose the number of linguistic variables.

Chapter 3

TWO AREA INTERCONNECTED POWER SYSTEMS & DYNAMIC MODEL

3.1 Introduction to Load Frequency Control

In this chapter, the basic idea about LFC and the physical model of interconnected two-area power systems are introduced. Each area of the power system consists of governor, turbine, and generator, which are explained in this chapter respectively. Two different kinds of turbines: reheat turbine, and hydro turbine, are discussed. The frequency error, tie-line power error and conventional area control error are defined. In addition, the block diagram of a nonlinear model for the two area interconnected power system is presented in this chapter.

A change in the power load can be reflected through the system frequency. The frequency is an important index for the generation and load imbalance. Any short imbalance can cause instantaneous frequency deviation until the load disturbance is offset by electric energy provided by generator. The control of frequency and power generation is referred to as load frequency control (LFC), which is a major part of the automatic generation control (AGC) [18].

Figure 3.1 shows the block diagram of a synchronous generator with basic frequency control loops. In Figure 3.1, ΔP_C is the output of the speed changer motor, ΔP_g is the output of the speed governor, Δf is the frequency error, ΔP_L is the load disturbance, w is the angular velocity, and ΔP_m is the mechanical power of the output of the turbine. As shown in this figure, the major parts of the frequency control loop are a speed changer motor, a speed governor, a hydraulic amplifier, a turbine, and a generator. The speed governor is used to sense the frequency change through the primary and secondary frequency control. Hydraulic amplifier provides the mechanical force to position the valve against the pressure of steam or water. It also provides the output power for the turbine. The output power of generator is controlled by the mechanical output of the turbine. The mechanical power of a turbine is controlled by the opening or closing of the valve which regulates steam or water to the turbine. Steam or water must constantly flow to the turbine to satisfy the load demand, otherwise the speed will vary and the frequency will continuously change [20].

In Figure 3.1, if there is a change in the load, the generation power will change in order to satisfy the load demand. The output of mechanical power from the turbine will vary accordingly to match the generation power. The output of speed governor changes accordingly. This constitutes the primary frequency control.

Primary frequency control is not enough for load frequency control due to its inability to restore the frequency. A supplemental frequency controller is needed to adjust the load reference point through the speed changer motor. The supplemental frequency control is also called LFC. In the LFC, the frequency deviation measured by a frequency sensor is added to the primary control loop through a controller. In reality, the controller could be an integral controller, PI and PID controller, or other advanced controllers. The output of the speed changer motor (ΔP_C) is used to regulate the frequency of the power system.

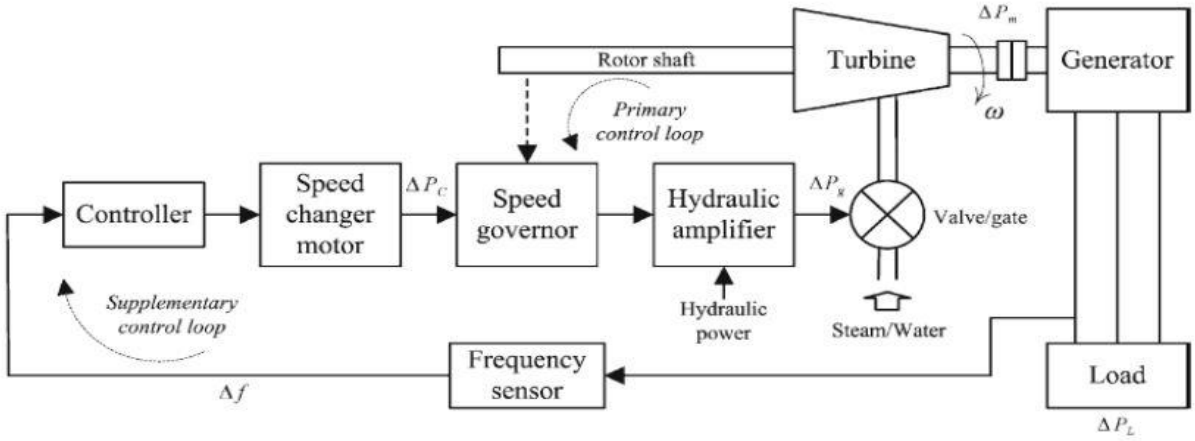

Figure 3.1 Block Diagram of a Synchronous Generator with Basic Frequency Control Loops [16]

3.2 Modeling of Power System Components

A conventional single-area power system is shown in Figure 3.2. The major parts are a speed changer, a speed governor, a hydraulic amplifier, and a control valve. They are connected by a linkage mechanism. In Figure 3.2, A , B , and C are in one linkage mechanism, C , D , and E are in another linkage mechanism, and P_{ref} is the output power of the turbine in steady state. When A moves downwards, B moves downwards; C moves upwards; D moves upwards; and E moves downwards. This allows more steam into the turbine and consequently results in more output generation power. High pressure oil is used to control the pilot valve. The main piston can move up and down depending on the position of E. The output of a speed governor is ΔP_g, which corresponds to the movement of ΔX_C as shown in Figure 3.2. The speed governor has two inputs: one is the reference input ΔP_{ref} as shown in Figure 3.2, and the other is frequency deviation. The parameters ΔX_A, ΔX_B, ΔX_C, ΔX_D, ΔX_E are the displacements of links A, B, C, D, E. They move in vertical directions. In reality, the movements are measured in millimeters, but we define the movements in p u MW (per unit megawatts).

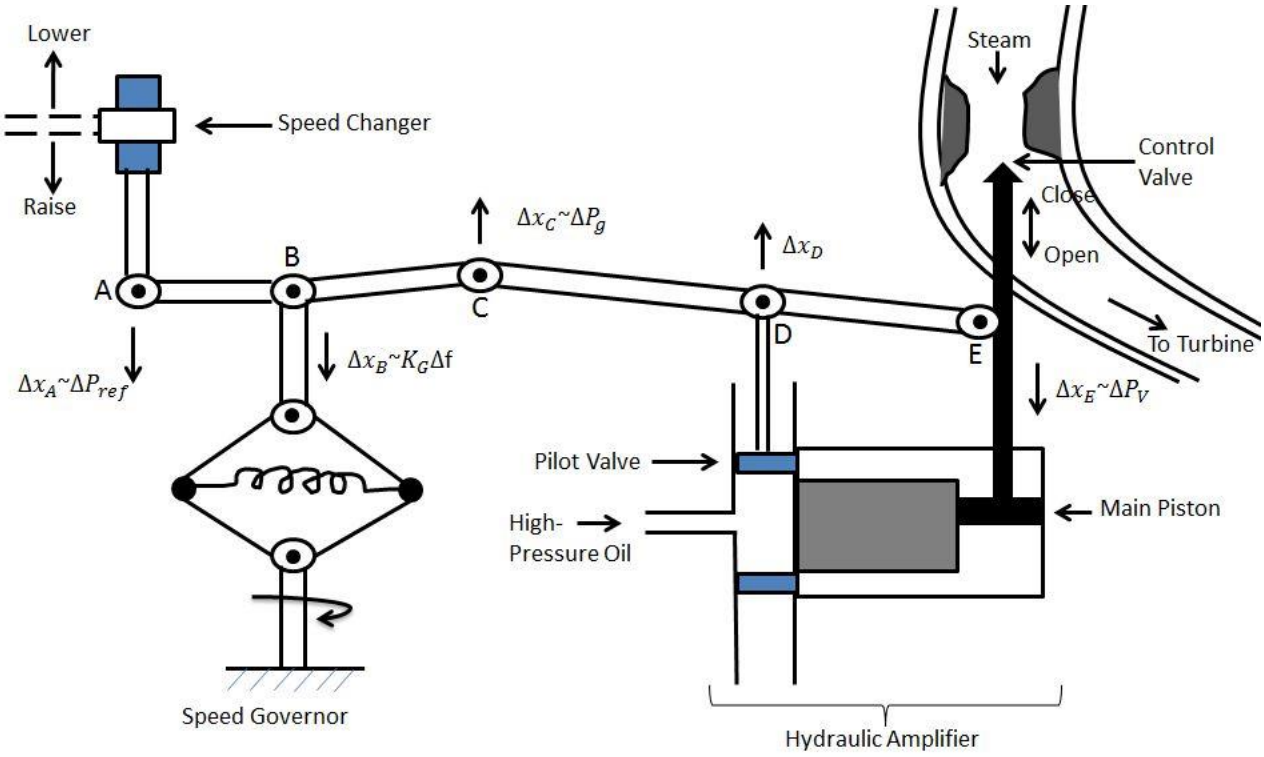

Figure 3.2 Conventional Single Area Power System [18]

3.2.1 Governor

As shown in Figure 3.2, "a positive ΔP_{ref} will cause positive ΔPg ". A positive Δf will cause linkage B and C to move down causing negative ΔP_g [38]." So we have

$$\Delta P_g = \Delta P_{ref} - \frac{1}{R}\Delta f \tag{3.1}$$

Where R is speed regulation of the governor and R has dimension of Hz /MW.
The Laplace transform of (3.1) can be written as

$$\Delta P_g(s) = \Delta P_{ref}(s) - \frac{1}{R}\Delta f(s) \tag{3.2}$$

The block diagram of (3.2) is shown in Figure 3.3.

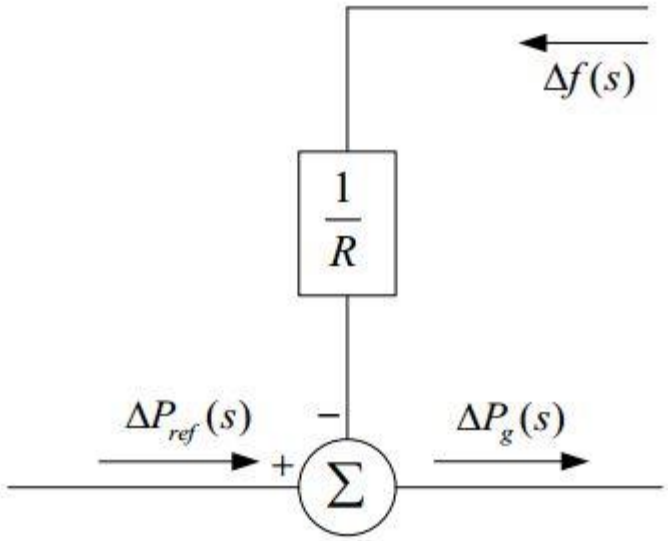

Figure 3.3 Block Diagram of Speed Governor

As shown in Figure 3.2, the output of the hydraulic actuator is ΔP_V, and the inputs to ΔX_D are ΔPg and ΔP_V . For a positive ΔPg , the change in ΔX_D must be positive. For a negative change in ΔP_V , the change in ΔX_D is positive. So we have

$$\Delta X_D = \Delta P_g - \Delta P_V \tag{3.3}$$

The relationship between the output and input of a hydraulic actuator is represented by

$$\Delta P_V = K_G - \int \Delta X_D dt \tag{3.4}$$

The Laplace transform of (3.3) and (3.4) can be written as (3.5) and (3.6)

$$\Delta X_D(s) = \Delta P_g(s) - \Delta P_V(s) \tag{3.5}$$

$$\Delta P_V(s) = \frac{K_G}{s} \Delta X_D(s) \tag{3.6}$$

Substituting (3.5) into (3.6) and eliminating the $\Delta X_D(s)$, we can get the relationship between $\Delta P_V(s)$ and $\Delta P_g(s)$ as

$$\Delta P_V(s) = \frac{1}{1+sT_G}\Delta P_g(s) \tag{3.7}$$

Where T_G is time constant, and it can be expressed as (3.8).

$$T_G = \frac{1}{K_G} \tag{3.8}$$

Usually T_G is around 0.1 sec. Equation (3.7) can be written as (3.9), where T_G represents the governor time constant for the power system with reheat turbine.

$$G_H(s) = \frac{\Delta P_v(s)}{\Delta P_g(s)} = \frac{1}{1+sT_G} \tag{3.9}$$

Combining (3.2) and (3.9), we obtain the block diagram of speed governor and hydraulic actuator as shown in Figure 3.4.

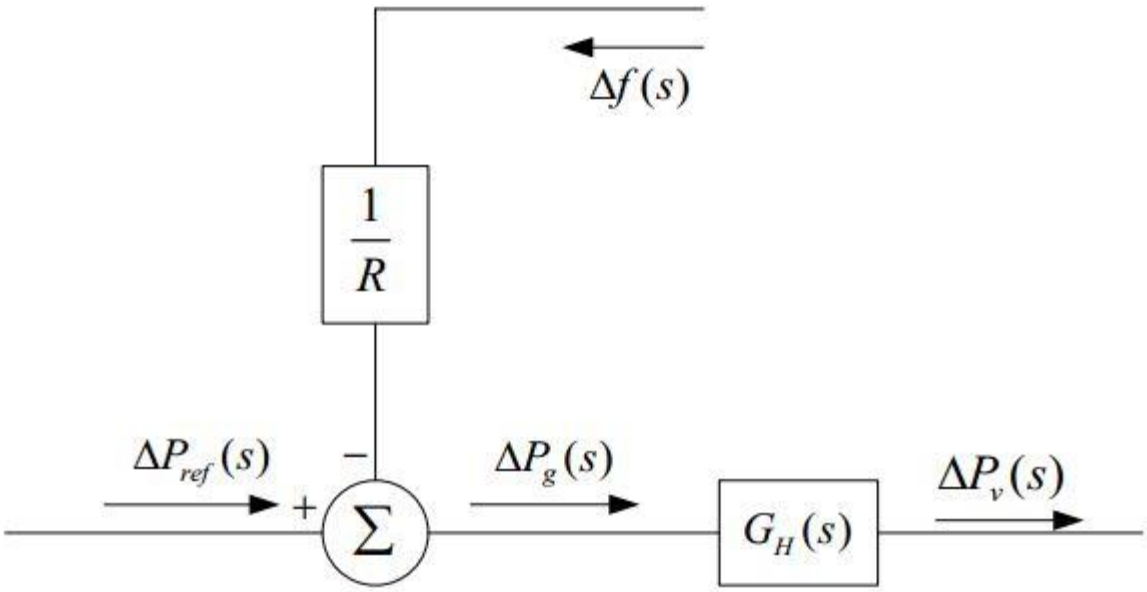

Figure 3.4 Block Diagram of Speed Governor and Hydraulic Valve Actuator

In reality, the governor is nonlinear, which includes dead band [25]. "By changing the input signal, the speed governor may not immediately react until the input reaches a specified value. This limitation called speed governor dead band. All governors have a dead band in response, which is important for power system frequency control in the presence of disturbances [26]."

Figure 3.5 shows the block diagram of the speed governor and hydraulic actuator with nonlinear part of the governor, which is dead band. The value of the dead band must be 0.036Hz for the frequency of power system operating at 50Hz according to North American Electric Reliability Corporation (NERC) rule [28].

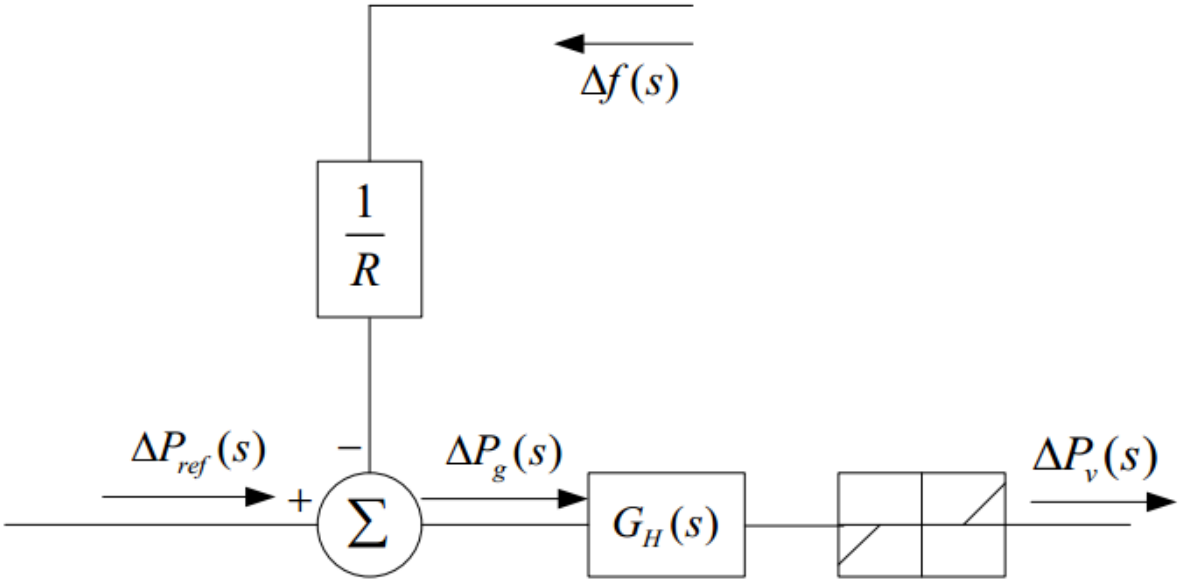

Figure 3.5 Block Diagram of Speed Governor and Hydraulic Valve Actuator with Dead Band

3.2.2 Turbine

In normal state, the turbine power P_T is in balance with the generation power P_G, resulting in zero accelerations, and constant speed and frequency [27]. The frequency deviation would be kept at zero. If the change in turbine power is ΔP_T and the change in generator power is ΔP_G [28], the accelerating power ΔP_A is

$$\Delta P_A = \Delta P_T - \Delta P_G \tag{3.10}$$

From (3.10), it can be clearly seen that if $\Delta P_A > 0$, the system will accelerate. If $\Delta P_A < 0$, the system will decelerate. The non-reheat turbine is shown in Figure 3.6. In Figure 3.6, steam passes through a valve and steam chest and enters the turbine. The steam chest is a device that contains control valves which regulate the flow of the steam into the turbine. Condenser is used to produce a vacuum at the turbine exhaust and to recover the condensed steam which can be used again.

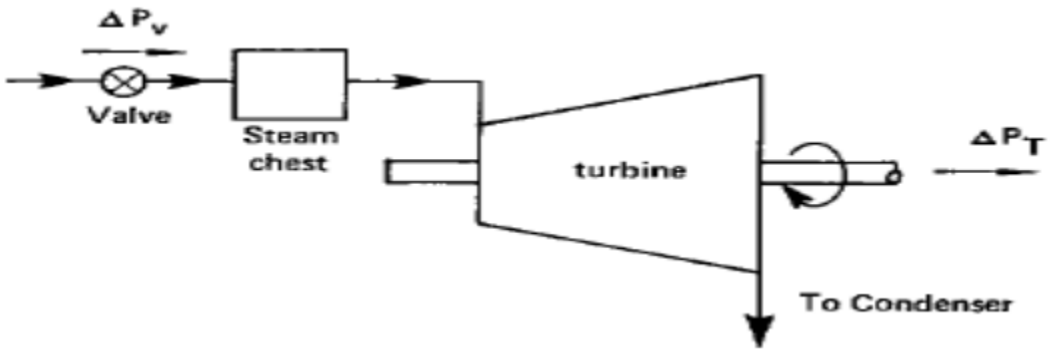

Figure 3.6 Non-reheat Turbine

The turbine power increment ΔP_T depends on the valve power increment ΔP_V and the type of turbine [28]. The transfer function of the non-reheat turbine between ΔP_T and ΔP_V is shown in (3.11) where G_T (s) is the transfer function for the non-reheat turbine ($G_T(s) = \frac{1}{1+sT_t}$) and T_t is the steam chest time constant.

$$\Delta P_T(s) = \Delta G_T(s)\Delta P_V(s) = \frac{1}{1+sT_t}\Delta P_V \tag{3.11}$$

The generated power change ΔP_G is equal to the load power change ΔP_D . So we have (3.12).

$$\Delta P_G(s) = \Delta P_D(s) \tag{3.12}$$

From (3.1) to (3.12), we have the graph shown in the Figure 3.7. In Figure 3.7, we add the transfer function of the turbine to Figure 3.4.

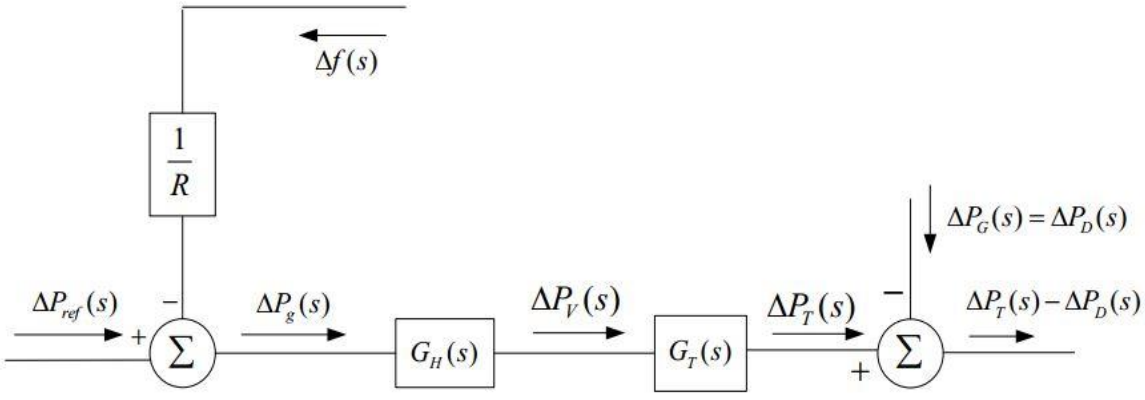

Figure 3.7 Block Diagram of Primary Loop of LFC

The reheat turbine is shown in Figure 3.8. There are two stages: high pressure (HP) and low pressure (LP) in reheat turbine. “The design increases efficiency and is always used for large units [29].”

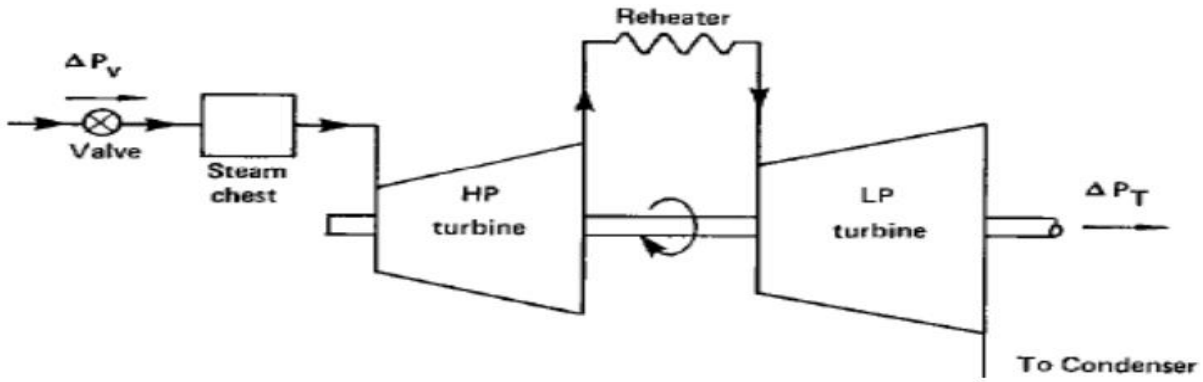

Figure 3.8 Reheat Turbine [27]

A hydro turbine is shown in Figure 3.9. The “head” is the “magnitude of the water.” The water is flowing through penstock from the “head”. The penstock creates water pressure through changing the vertical drop.

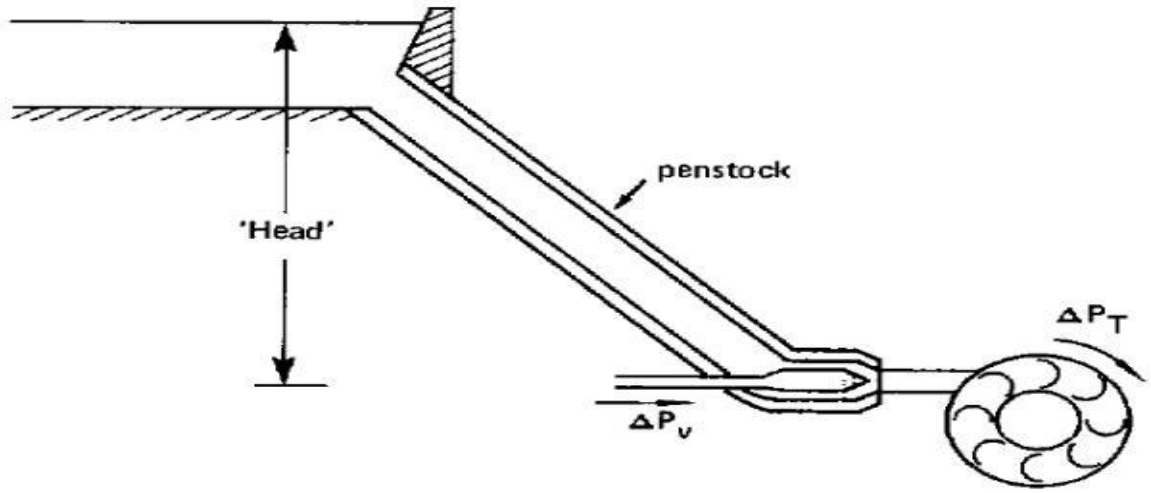

Figure 3.9 Hydro Turbine

The transfer function $G_T(s)$ for a non-reheat turbine (in Figure 3.6) is expressed in (3.13), where T_t is the steam chest time constant. Typically, $100 \leq T_t \leq 500$ [ms] .

$$G_T(s) = \frac{1}{1+sT_t} \tag{3.13}$$

The reheat turbine is shown in Figure 3.8. The high pressure contributes to the power component as shown in (3.14).

$$\Delta P_{THP}(s) = \frac{K_R}{1+sT_t}\Delta P_V(s) \tag{3.14}$$

Where $\Delta P_{THP}(s)$ is the transfer function for the high pressure stage of the reheat turbine, and K_R is the high pressure rating. The low pressure contributes to the power component as shown in (3.15).

$$\Delta P_{TLP}(s) = \frac{1-K_R}{(1+sT_t)(1+sT_{RH})}\Delta P_V(s) \tag{3.15}$$

Where $\Delta P_{TLP}(s)$ is the transfer function for the low pressure stage of the reheat turbine, T_{RH} is the delay time between high pressure stage and low pressure stage, and $4 \leq T_{RH} \leq 10$[s].

The total output of reheat turbine is the sum of the outputs for low pressure and high pressure stages as shown in (3.16), where $G_{TRH}(s)$ is the transfer function for the reheat turbine.

$$G_{TRH}(s) = \frac{1+sK_RT_{RH}}{(1+sT_t)(1+sT_{RH})} \tag{3.16}$$

The transfer function for the hydro turbine is shown in (3.17), where T_W is the time that it takes for the water to pass through the penstock. The hydro turbine system is not stable, because it has a positive zero, which is $s = \frac{1}{T_W}$

$$G_T(s) = \frac{1-sT_W}{1+0.5sT_t} \tag{3.17}$$

For the hydro turbine, there is transient response coefficient. The transient response coefficient function is as shown in (3.18), where T_R is reset time, ΔR_T is temporary droop coefficient, ΔRP is permanent droop coefficient, and $T_2 = R_T T_R / R_p$.

$$G_{TRC}(s) = \frac{1+T_R s}{1+(R_T / R_P)sT_R} = \frac{1+T_R s}{1+T_2 s} \tag{3.18}$$

The equations (3.13), (3.16), and (3.17) just represent the linear parts of turbines. In practice, there exists the maximum and minimum limit on the rate of change in the generating power [30]. Therefore, GRC has to be included in the turbine systems. Figure 3.10 shows the nonlinear turbine model with GRC. A typical value for GRC with thermal units is 3%/min, which is bounded by ±0.0005 for the AGC to preventexcessive control. For a hydraulic turbine, the GRC is bounded by ±0.0045 for the raising generation and ±0.06 for the lowering generation [29].

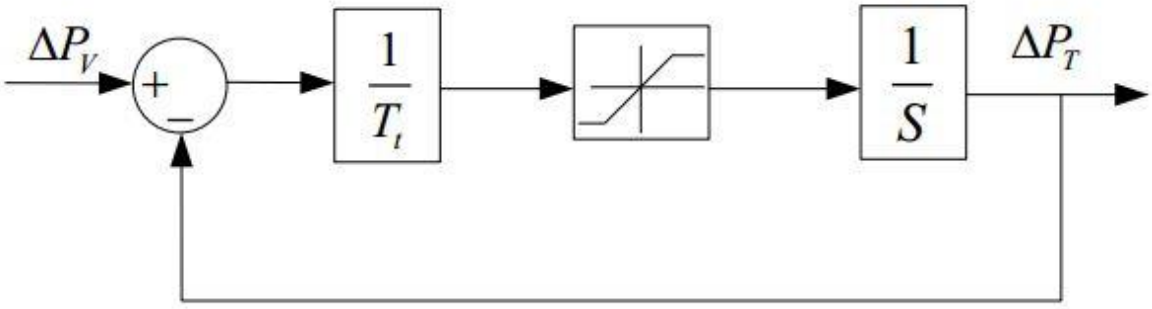

Figure 3.10 Nonlinear Turbine Model with Generation Rate Constraint

3.2.3 Generator

The power system is originally in balance, and the frequency of power system is at its normal value which is 60Hz in North America. The kinetic energy of rotating equipment is represented by W^0_{Kin} MW sec. If the load is increased by ΔP_D , the generation will increase by ΔP_G to match the load increases as shown in (3.12) [28].

However, it usually takes some time for the control valve to act and increase the turbine power. The increase in turbine power is not equal to generation power. So there is a power imbalance that is ΔP_T - ΔP_G. As a result, the speed and frequency will change. The kinetic energy is proportional to the square of

the speed as shown in (3.19) where f^0 is the normal frequency, f is the real frequency, and W^0_{Kin} is rated kinetic energy [28].

$$W_{Kin} = W^0_{Kin}(\frac{f}{f^0})^2 MW\sec \tag{3.19}$$

The load change over frequency change can be written as (3.20), where D is demanding coefficient.

$$D = \frac{\partial P_D}{\partial f} MWH \tag{3.20}$$

So we have

$$\Delta P_T - \Delta P_D = \frac{d}{dt}(W_{Kin}) + D\Delta f \tag{3.21}$$

Where Δf is the frequency deviation and $f = f^0 + \Delta f$ From (3.19), we have

$$W_{Kin} = W^0_{Kin}(\frac{f^0 + \Delta f}{f^0})^2 = W^0_{Kin}[1 + \frac{2f^0\Delta f}{f^0} + (\frac{\Delta f}{f^0})^2] \approx W^0_{Kin}(1 + \frac{2f^0\Delta f}{f^0})MW\sec \tag{3.22}$$

The derivative of W_{Kin} is given in (3.23)

$$\frac{d}{dt}(W_{Kin}) = \frac{2W^0_{Kin}}{f^0}\frac{d}{dt}\Delta f \tag{3.23}$$

Substituting (3.23) into (3.21), we have (3.24).

$$\Delta P_T - \Delta P_D = \frac{2W^0_{Kin}}{f^0}\frac{d}{dt}(\Delta f) + D\Delta f \tag{3.24}$$

The per unit inertial constant H is given as (3.25), where P_r is the generator rating

$$H = \frac{W_{Kin}^{0}}{P_r} \sec \tag{3.25}$$

Substituting (3.25) into (3.24), we have (3.26)

$$\Delta P_T - \Delta P_D = \frac{2HP_r}{f^0}\frac{d}{dt}(\Delta f) + D\Delta f \quad puMW \tag{3.26}$$

The Laplace transform of (3.26) is shown in (3.27)

$$\Delta P_T(s) - \Delta P_D(s) = \frac{2HP_r}{f^0} s \frac{d}{dt}\Delta f(s) + D\Delta f(s) \tag{3.27}$$

From (3.27), Δf (s) can be derived as shown in (3.28)

$$\Delta f(s) = \frac{1}{\frac{2HP_r}{f^0}s + D}[\Delta P_T(s) - \Delta P_D(s)] \tag{3.28}$$

Equation (3.28) can be rewritten as

$$\Delta f(s) = G_P(s)[\Delta P_T(s) - \Delta P_D(s)] \tag{3.29}$$

In (3.29), $G_P(s)$ is given by (3.30)

$$G_P(s) = \frac{1}{\frac{2HP_r}{f^0}s + D} = \frac{1/D}{1 + \frac{2HP_r}{Df^0}s} = \frac{K_P}{1 + sT_P} \tag{3.30}$$

Where Kp= 1/D and TP = 2HPr/Df0

Equation (3.30) represents the missing link in the feedback path in Figure 3.7. When (3.30) is added to the system, the loop becomes closed as shown in Figure 3.11.

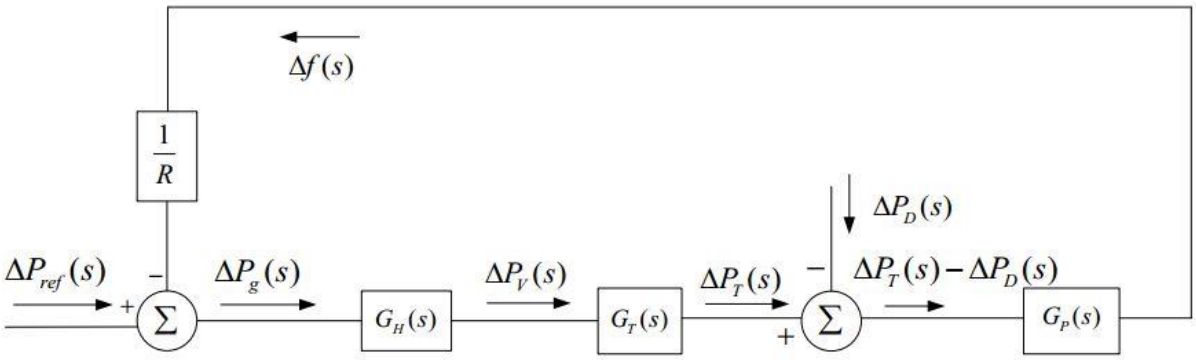

Figure 3.11 Block Diagram of Closed Loop Primary LFC

For the generator, we generally use a linear model to represent it. The nonlinear part of a generator can be ignored due to its small impact on the power system compared to the nonlinear parts associated with governors and turbines.

Any power system operates within prescribed voltage and frequency limits. System operators maintain the frequency within strict limits. The steady state frequency error must be maintained at zero. In order to maintain the frequency error to be zero, the speed changer must be adjusted automatically according to the frequency changes. So in this case, an integral control is introduced. The frequency error is amplified and then integrated. The signal ΔP_{ref} is negative because a negative frequency error will raise the command as shown in (3.31), where K_1 is controller gain constant [27]

$$\Delta P_{ref} = -K_1 \int \Delta f dt \tag{3.31}$$

The Laplace transform of (3.31) is shown in (3.32)

$$\Delta P_{ref}(s) = -\frac{K_1}{s} \Delta f(s) \tag{3.32}$$

The frequency error is fed into the integrator and its output is used to control speed changer position. Figure 3.12 shows the block diagram of complete LFC with an integral controller added to the loop.

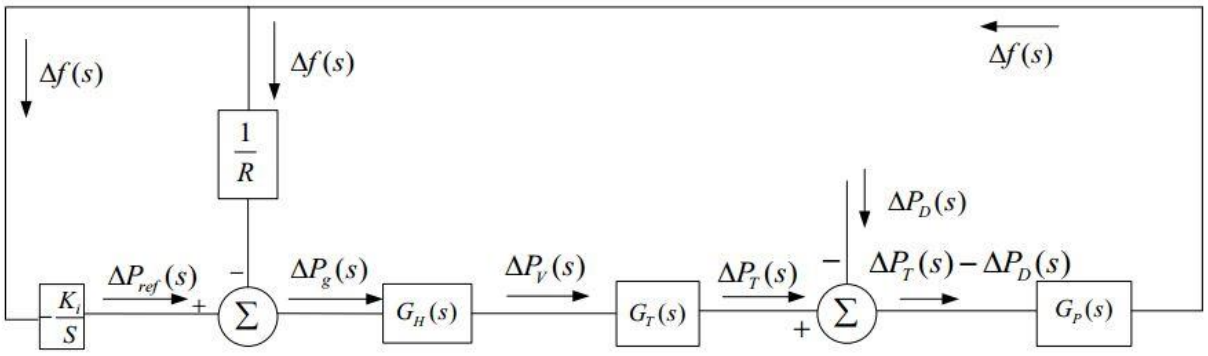

Figure 3.12 Block Diagram of Complete LFC System with Integral Controller

From Figure 3.12, we can see that if frequency error is nonzero, the output of the integral controller will increase. It will also result in the moving of speed changer because the output of integral control is connected to the speed changer as shown in Figure 3.1. When the frequency error is maintained at zero, the output of integrator will be zero as well. Then the speed changer position remains at a constant value [28].

3.3 Tie-Line Power Error

The frequency error must be kept zero. In addition, "a static error in tie-line power flow would mean that one area would have to support the other on a steady state basis [26]." In normal conditions, the power flow through the tie-line connecting area i and area j is given by (3.33).

$$P_{ij} = \frac{|V_i||V_j|}{X}\sin(\delta_i^0 - \delta_j^0) \tag{3.33}$$

In (3.33), V_i and V_j are the voltages in area i and area j respectively and δ^0_i , δ^0_j are the angles of the voltages in area i and area j respectively.

For small changes in the angels δ^0_i and δ^0_j , the tie line power change ΔP_{ij} can be written as

$$\Delta P_{ij} = \frac{|V_i||V_j|}{X}\cos(\delta_i^0 - \delta_j^0)(\delta_i - \delta_j) \tag{3.34}$$

We define the synchronizing coefficient as

$$T_0 = \frac{|V_i||V_j|}{X}\cos(\delta_i^0 - \delta_j^0) \quad MW/rad \tag{3.35}$$

Then (3.34) can be expressed as

$$\Delta P_{ij} = T_0(\delta_i - \delta_j) \quad MW \tag{3.36}$$

The relationship between frequency f and angular frequency w can be expressed as (3.37), where δ_s is the angle.

$$f = \frac{w}{2\pi} = \frac{1}{2\pi}\frac{d\delta_s}{dt} \tag{3.37}$$

From (3.37), we will have

$$\delta_s = 2\pi\int_0^t f dt \tag{3.38}$$

Equation (3.36) can be written in terms of frequency deviations Δf_1 and Δf_2 as shown in (3.39)

$$\Delta P_{ij} = 2\pi T_0(\int_0^t \Delta f_i dt - \int_0^t \Delta f_j dt) \tag{3.39}$$

The Laplace transform of (3.39) can be written as (3.40)

$$\Delta P_{ij} = \frac{2\pi T_0}{s}[\Delta f_1(s) - \Delta f_2(s)] \tag{3.40}$$

Equation (3.40) can be represented by the block diagram shown in Figure 3.13

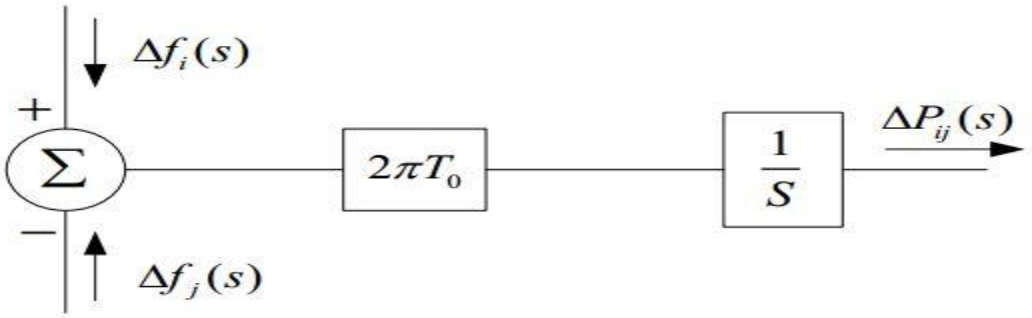

Figure 3.13 Block Diagram of Tie-line Power Error

3.4 Area Control Error

The frequency error and tie-line power error must be kept at zero. So, one objective of LFC is to maintain the frequency of power system at 50Hz with a tolerance of 0.5Hz. The other objective is to maintain the scheduled power interchange in an interconnected power system[24]. To meet the objectives, a conventional ACE has been introduced. The conventional ACE is defined as a linear combination of frequency error and tie-line power error. The equation for ACE is shown in (3.41) where B_i is thefrequency response coefficient in area i .

$$ACE_i = \sum_{j=1,2...n,\, i \neq j} \Delta P_{ij} + B_i \Delta f_i \tag{3.41}$$

From (3.41), we can see that as long as ACE is zero, both tie line power change and frequency error will be zero as well. Therefore our control goal is to force the ACE to zero.

3.5 Two Area Interconnected Power System

The block diagram of a nonlinear, two-area interconnected power system is shown in Figure 3.14 reheat turbine, and hydro turbine are distributed in two areas respectively. The nonlinearities such as governor dead band and GRC are included in the model. In Figure 3.14, ΔP_{Li} is the load disturbance in area i (i = 1,2) , Δf_i is the frequency error in area i , ΔP_{tiei} is the tie-line power change between area i and the other area, ACEi is the area control error in area i , u_i is the control input in area i , B_i is the frequency response

coefficient of area i , R_i is the speed droop coefficient of area i , T_{ij} is the tie-line coefficient between area i and area j, ΔX_{gi} is the valve/gate position change for the power system in area i ,ΔP_{gi} is the mechanical power for the power system in area i , ΔX_{gh} and ΔX_{gr} are intermediate variables, K_{pi} is power system gain constant for area i , T_{pi} is time constant for area i , K_r is reheat coefficient, T_r is reheat time constant, T_{ti} is the steam chest time constant, T_{Gi} represents the time constants for the governors in area i , T_R is reset time, and T_W is the time that it takes for the water to pass through a penstock. In addition, The area with reheat turbine is defined as area 1. The area with hydraulic turbine is defined as area 2.

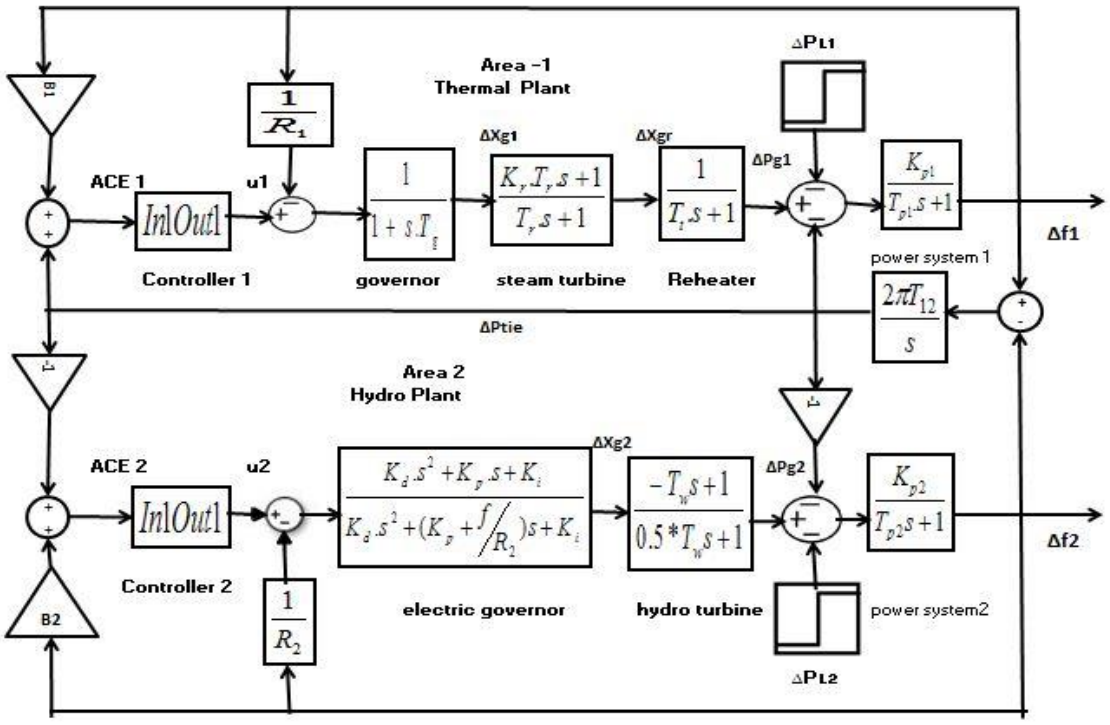

Figure 3.14 Block diagram of a nonlinear two-area interconnected power system

3.6 Mathematical Model of Two-Area Interconnected Power System

In this section, the models of two areas with different turbines including reheat, and hydraulic turbines are developed respectively. We will start with the area 1 which contains reheat turbine. From (3.30), the relationship between the mismatch power (ΔPg1- ΔPtie - ΔP_{L1}) and the frequency error Δf_1 can be expressed as

$$\Delta \dot{f}_1 = (\frac{K_{p1}}{T_{p1}})(\Delta P_{g1} - \Delta P_{tie1} - \Delta P_{L1}) - (\frac{1}{T_{p1}})\Delta f_1 \tag{2.42}$$

From (3.16), we can obtain the following two equations where ΔX_{gr} is a medium variable

$$\frac{\Delta P_{g1}}{\Delta X_{gr}} = \frac{1 + K_r T_r s}{1 + T_r s} \tag{3.43}$$

$$\frac{\Delta X_{gr}}{\Delta X_{g1}} = \frac{1}{1 + T_{t1} s} \tag{3.44}$$

From (3.43), ΔP_{g1} can be expressed as

$$\Delta \dot{P}_{g1} = \frac{1}{T_r}(\Delta X_{gr} + K_r T_r \Delta \dot{X}_{gr} - \Delta P_{g1}) \tag{3.45}$$

From (3.44), ΔX_{gr} can be expressed as

$$\Delta \dot{X}_{gr} = \frac{1}{T_{t1}} \Delta X_{g1} - \frac{1}{T_{t1}} \Delta X_{gr} \tag{3.46}$$

Substituting (3.46) into (3.45), we obtain an ODE model to express the relationship between mechanical power for area 1 and media part ΔX_{gr} in area 1. The ODE model is given by

$$\Delta \dot{P}_{g1} = \frac{1}{T_r} \Delta X_{gr} + \frac{K_r}{T_{t1}} \Delta X_{g1} + \frac{K_r}{T_{t1}} \Delta X_{gr} - \frac{1}{T_r} \Delta P_{g1} \tag{3.47}$$

From (3.9), we can obtain an ODE model to represent the relationship between control input, frequency error, and valve/gate position change in area 1. The ODE model is given by

$$\Delta \dot{X}_{g1} = \frac{1}{T_{g1}} u_1 - \frac{1}{R_1 T_{g1}} \Delta X_{g1} - \frac{1}{T_{g1}} \Delta X_{g1} \tag{3.48}$$

From (3.40), the tie-line power in area 1 can be calculated as

$$\Delta \dot{P}_{tie1} = 2\pi T_{12} \left(\Delta f_1 - \Delta f_2 \right) \tag{3.49}$$

Finally, we develop the mathematical model for area 2. From (3.30), the relationship between the mismatch power (ΔP_{g2}- ΔP_{tie2} - ΔP_{L2}) and the frequency error (Δf_2) can be expressed as

$$\Delta \dot{f}_2 = (\frac{K_{p2}}{T_{p2}})(\Delta P_{g2} - \Delta P_{tie2} - \Delta P_{L2}) - (\frac{1}{T_{p2}})\Delta f_2 \tag{3.50}$$

From (2.9), (2.17) and (2.18), we can get the ODE model for the mechanical power in area 2.

$$\Delta \dot{P}_{g2} = \frac{2\Delta X_{g2}}{T_W} - \frac{2\Delta X_{gh}}{T_1} - \frac{2T_R u_2}{T_1 T_{g2}} + \frac{2T_R \Delta f_2}{T_1 R_2 T_{g2}} + \frac{2T_R \Delta X_{gh}}{T_1 T_{g2}} + \frac{2\Delta X_{g2}}{T_1} - \frac{2\Delta P_{g2}}{T_W} \tag{3.51}$$

From (3.9) and (3.18), the derivative of the valve/gate position in area 2 can be expressed as

$$\Delta \dot{X}_{g2} = \frac{\Delta X_{gh}}{T_1} + \frac{T_R u_2}{T_1 T_{g2}} - \frac{T_R \Delta f_2}{T_1 R_2 T_{g2}} - \frac{T_R \Delta X_{gh}}{T_1 T_{g2}} - \frac{\Delta X_{g2}}{T_1} \tag{3.52}$$

From (3.9), the relationship between control input, frequency error, and valve/gate position change in area 2 can be expressed as

$$\Delta \dot{X}_{gh} = \left(\frac{1}{T_{g2}} \right) u_2 - \left(\frac{1}{T_{g2} R_2} \right) \Delta f_2 - \left(\frac{1}{T_{g2}} \right) \Delta X_{gh} \tag{3.53}$$

From (3.40), the tie-line power in area 2 can be calculated as

$$\Delta \dot{P}_{tie2} = 2\pi T_{21} \left(\Delta f_2 - \Delta f_1 \right) \tag{3.54}$$

Chapter 4

VARIABLE STRUCTURE BASED SLIDING MODE INTELLIGENT LOAD FREQUENCY CONTROL

In this chapter, we introduce a variable structure based sliding mode controller firstly and then apply the sliding mode control technology to the two areas of an interconnected power system respectively.

4.1 Introduction of Sliding Mode Control

Sliding mode control (SMC) has been successfully applied in a wide spectrum of systems including multi-input and multi-output systems, nonlinear systems, discrete systems, large scale and infinite-dimension systems [29]. SMC is a kind of robust control method. The major advantage of sliding mode control is that it is insensitive to the plant parameter variations and disturbances. Variable structure based SMC is capable of decoupling high order systems into low order systems, which reduces the complexity of feedback design. Also, SMC is suitable for nonlinear systems, high order systems, and complex systems. SMC has been proven to be applicable in a large scope of problems, such as robotics, electric drives, process control, and vehicle and motion control [28].

Variable structure control (VSC) is a form of discontinuous nonlinear control. The method alters the dynamics of a nonlinear system by application of a high-frequency switching control. The state-feedback control law is not a continuous function of time; it switches from one smooth condition to another. So the structure of the control law varies based on the position of the state trajectory; the method switches from one smooth control law to another and possibly very fast speeds (e.g., for a countably infinite number of times in a finite time interval). The main mode of VSC operation is sliding mode control (SMC). The strengths of SMC include:

- Low sensitivity to plant parameter uncertainty
- Greatly reduced-order modeling of plant dynamics
- Finite-time convergence (due to discontinuous control law)

In control system, sliding mode control, or SMC, is a nonlinear control method that alters the dynamics of a nonlinear system by application of a discontinuous control signal that forces the system to "slide" along a cross-section of the system's normal behavior. The state-feedback control law is not a continuous

function of time. Instead, it can switch from one continuous structure to another based on the current position in the state space. Hence, sliding mode control is a variable structure control method. The multiple control structures are designed so that trajectories always move toward an adjacent region with a different control structure, and so the ultimate trajectory will not exist entirely within one control structure. Instead, it will slide along the boundaries of the control structures. The motion of the system as it slides along these boundaries is called a sliding mode and the geometrical locus consisting of the boundaries is called the sliding (hyper) surface. In the context of modern control theory, any variable structure system, like a system under SMC, may be viewed as a special case of a hybrid dynamical system as the system both flows through a continuous state space but also moves through different discrete control modes.

Variable structure based SMC consists of three parts: a sliding surface, switching control, and equivalent control. The sliding surface contains the desired state trajectories. Switching control is a discontinuous control law to drive system states to converge to the sliding surface. Equivalent control is a continuous control law to force the system states to remain on the surface [30].

The purpose of SMC is to drive the plant trajectory to a sliding surface and to maintain the trajectory on the sliding surface in subsequent time. The first step of designing a SMC is to select a sliding surface. The feedback controller has different controller gains depending on whether a system's trajectory is above or below the surface. Consider a nonlinear system, which can be defined as (4.1).

$$x^n = f(x, \dot{x}, \ddot{x}, \dddot{x}, x^{(n-1)}, t) + b(x,t)u(t) \tag{4.1}$$

In (4.1), x (t) is the state vector, n indicates the highest order of the system, *f (x , t)* and *b(x ,t)* are nonlinear functions of time and state, and u(t) is the control input. The sliding surface is defined as

$$s(x,t) = \left(\frac{d}{dt} + \delta\right)^{(n-1)} \tilde{x}(t) \tag{4.2}$$

where δ is a strict positive constant, and $\tilde{x}(t)$ is the error between the output state x(t) and desired output $x_d(t)$.

For a second order system, the sliding surface will be $s = \dot{e} + ce$, where e is the tracking error between the output state and desired output. The demonstration of sliding surface in phase plane is presented in Figure 4.1. In Figure 4.1, SMC should force any initial states to land on the sliding surface in a finite

time. If both the tracking error and the derivative of the tracking error are zero, the system states reach the demanded states [30]. In Figure 4.1, the slope of the sliding surface, which is c, is a constant. So if s=0, the system states will reach the demand states.

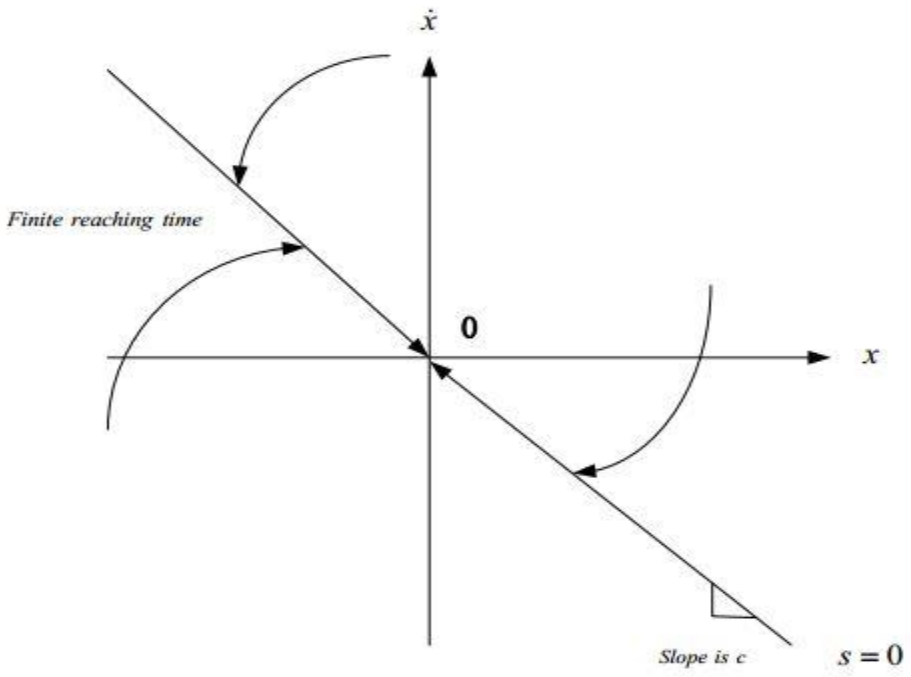

Figure 4.1 Sliding Surface

After the sliding surface is defined, the switch control law is used to force the system states to land on the sliding surface even if there is a disturbance. The switching law can be defined as (4.3), where u is switching control law, u0 is the positive control gain, and s is the sliding surface. The switching law has two outputs depending on the sign of the sliding surface. If the sliding surface is positive, the switching control law is positive and vice versa [29].

Parameters used in this chapter shown in Table 4.1.

TABLE 4.1 PARAMETERS USED FOR LOAD FREQUENCY CONTROLLER

Parameters	Values
f	50 Hz
$R_1 = R_2$	2.5 Ω/ p.u. MW
$Dg_1 = Dg_2$	8.33 X 10^{-3} per unit MW/Hz
Tsg	0.075 sec
Tsp	20 sec
T_{12}	0.0707 MW/rad
Ptie.max	250 MW
K_d	5.0
Trc	10 sec
Krc	0.5
$Hg_1 = Hg_2$	5 sec
$Par_1 = Par_2$	2000MW
$K_{P1}=K_{P2}$	120 Hz p.u./MW
$B_1=B_2$	0.25
T_{st}	0.33 sec
T_{wh}	1.2 sec
K_i	4.0

The equivalent control is used to keep the system states on the sliding surface. The equivalent control law can compensate system uncertainties. Differentiating the sliding surface (4.2) yields

$$\dot{s}(x,t) = f(x,\dot{x},\ddot{x},\dddot{x},x^{(n-1)},t) + b(x,t)u(t) - x_d^n(t) + \delta^n x(t) - \delta^n x_d(t) + ... \tag{4.4}$$

In (4.4), the omitted part represents the lower-order nonlinear systems given by (4.1), the highest order of which is ranging from 1 to n-1. We define the estimate of $f(x,\dot{x},\ddot{x},\dddot{x},x^{(n-1)},t)$ as $\hat{f}(x,\dot{x},\ddot{x},\dddot{x},x^{(n-1)},t)$.

In order to make the derivative of sliding surface zero, we have to choose the equivalent control input $\hat{u}(t)$ as

$$\hat{u}(t) = -\frac{1}{b(x,t)}\hat{f}(x,\dot{x},\ddot{x},\dddot{x},x^{(n-1)},t) + \frac{1}{b(x,t)}[x_d^n(t) - \delta^n x(t) + \delta^n x_d(t) + ...] \tag{4.5}$$

The omitted part in (4.5) is same as the one in (4.4). The stability of SMC is tested using Lyapunov's direct method. Define a positive definite Lyapunov function V(s) as (4.6), where s is the sliding surface. If the derivative of (4.6) is negative definite, the system will be asymptotically stable.

$$V(s) = \frac{1}{2} s^2 \geq 0 \tag{4.6}$$

The sliding mode control law (or the real control law u_{real}) is a linear combination of switch control law and equivalent control law. It is represented by

$$u_{real}(t) = -\frac{1}{b(x,t)} \hat{f}(x, \dot{x}, \ddot{x}, \dddot{x}, x^{(n-1)}, t) + \frac{1}{b(x,t)}[x_d^n(t) - \delta^n x(t) + \delta^n x_d(t) + ...] - \frac{k}{b(x,t)} \mathrm{sgn}(s(t)) \tag{4.7}$$

Replacing the u(t) in (4.4) with $u_{real}(t)$ in (4.7), we can obtain

$$\dot{s}(x,t) = f(x, \dot{x}, \ddot{x}, \dddot{x}, x^{(n-1)}, t) +$$

$$b(x,t)[-\frac{1}{b(x,t)} \hat{f}(x, \dot{x}, \ddot{x}, \dddot{x}, x^{(n-1)}, t) + \frac{1}{b(x,t)}[x_d^n(t) - \delta^n x(t) + \delta^n x_d(t) + ...] - \frac{k}{b(x,t)} \mathrm{sgn}(s(t))]$$
$$- x_d^n(t) + \delta^n x(t) - \delta^n x_d(t) + ... \tag{4.8}$$

We suppose $\hat{f}(x, \dot{x}, \ddot{x}, \dddot{x}, x^{(n-1)}, t)$ $(or\ \hat{f})$ is an accurate estimation of $f(x, \dot{x}, \ddot{x}, \dddot{x}, x^{(n-1)}, t), \quad i.e. f \approx \hat{f}$. Substituting (3.8) into the derivative of Lyapunov function we will get

$$\dot{V}(s) = \frac{1}{2} \frac{d}{dt} (s(t))^2 = -k \, \mathrm{sgn}(s) s \tag{4.9}$$

If k is chosen large enough, equation (4.10) will be satisfied. Hence the stability of SMC is proved.

$$-k \, \mathrm{sgn}(s(t)) s \leq -k|s(t)| \tag{4.10}$$

Based on the equation development above, we design SMCs to control the two interconnected areas with reheat, and hydraulic turbines respectively. Our control goal is to drive the frequency error, tie-line power error, and area control error (ACE) to zero in these areas.

4.2 Application of SMC to Two-Area Interconnected Power Systems

In this section, VSC-SMC is applied to the two area interconnected power system. Each area consists of a governor, a turbine, and a generator. However, each area contains different kind of turbines which are reheat steam turbine and hydro turbine.

4.2.1 SMC for the Area with Reheat Steam Turbine

In this section, VSC-SMC is applied to the power area with a reheat steam turbine (area 2 in Figure 4.14). We set the frequency error for the power system with a reheat turbine as Δx_1 .

$$\Delta f_1 = \Delta x_1 \tag{4.11}$$

From (3.30), the relationship between the frequency error and the mismatched power in area 2 is derived as

$$(\Delta P_{g1} - \Delta P_{L1} - \Delta P_{tie1}) \frac{K_{p1}}{T_{p1}s + 1} = \Delta x_1 \tag{4.12}$$

The ODE model of (4.12) is

$$\Delta P_{g1} = \Delta P_{L1} + \Delta P_{tie1} + \frac{T_{p1}}{K_{p1}} \Delta \dot{x}_1 + \frac{1}{K_{p1}} \Delta x_1 \tag{4.13}$$

From (3.47), we have

$$\frac{1 + sK_r T_r}{1 + sT_r} \Delta X_{gr} = \Delta P_{g1} \tag{4.14}$$

The ODE model of (4.14) is

$$\Delta \dot{P}_{g1} = \frac{1}{T_r}\Delta X_{gr} + \frac{K_r}{T_{t1}}\Delta X_{g1} - \frac{K_r}{T_{t1}}\Delta X_{gr} - \frac{1}{T_r}\Delta P_{g1} \tag{4.15}$$

Substituting (4.13) into (4.15), we have

$$\Delta \ddot{x}_1 = \frac{K_{p1}}{T_{p1}}\left(\frac{1}{T_r}\Delta X_{gr} + \frac{K_r}{T_{t1}}\Delta X_{g1}\right) - \frac{K_{p1}K_r}{T_{p1}T_{t1}}\Delta X_{gr} - \frac{K_{p1}}{T_{p1}T_r}(\Delta P_{L1} + \Delta P_{tie1})$$

$$-\frac{K_{p1}}{T_{p1}T_r}\left(\frac{T_{p1}}{K_{p1}}\Delta \dot{x}_1 + \frac{1}{K_{p1}}\Delta x_1\right) - \frac{K_{p1}}{T_{p1}}\left(\Delta \dot{P}_{L1} + \Delta \dot{P}_{tie1} + \frac{1}{K_{p1}}\Delta \dot{x}_1\right) \tag{4.16}$$

From (3.48), the relationship between valve/gate position change and the intermediate variable ΔXgr is shown as

$$\left(\Delta X_{g1} - \Delta X_{gr}\right)\frac{1}{T_{t1}}\frac{1}{s} = \Delta X_{gr} \tag{4.17}$$

The ODE model of (4.17) is

$$\Delta X_{g1} = T_{t1}\Delta \dot{X}_{gr} + \Delta X_{gr} \tag{4.18}$$

From (4.15), we get

$$\Delta X_{gr} = \frac{1}{1 + sK_rT_r}(T_r\Delta P_{g1}s + \Delta P_{g1}) \tag{4.19}$$

From (4.12), we have

$$\Delta P_{g1} = \Delta P_{L1} + \Delta P_{tie1} + \frac{T_{p1}}{K_{p1}}\Delta x_1 s + \frac{1}{K_{p1}}\Delta x_1 \tag{4.20}$$

Substituting (4.20) into (4.19), we have

$$\Delta X_{gr} = \frac{1}{1+sK_rT_r}(T_r\Delta P_{L1}s + T_r\Delta P_{tie1}s + \frac{T_rT_{p1}}{K_{p1}}\Delta x_1 s^2 + \frac{T_r}{K_{p1}}\Delta x_1 s + \Delta P_{L1}$$

$$+ \Delta P_{tie1} + \frac{T_{p1}}{K_{p1}}\Delta x_1 s + \frac{1}{K_{p1}}\Delta x_1) \tag{4.21}$$

From (4.17), we have

$$\Delta X_{g1} = T_{t1}\Delta X_{gr}\, s + \Delta X_{gr} \tag{4.22}$$

Replacing the ΔXgr in (4.22) with (4.21), we get

$$\Delta X_{g1} = \frac{1}{1+sK_rT_r}\{\frac{T_rT_{p1}T_{t1}}{K_{p1}}\Delta x_1 s^3 + (\frac{T_{t1}T_{p1}}{K_{p1}} + \frac{T_rT_{p1}}{K_{p1}} + \frac{T_rT_{t1}}{K_{p1}})\Delta x_1 s^2$$

$$+ (\frac{T_{t1}}{K_{p1}} + \frac{T_r}{K_{p1}} + \frac{T_{p1}}{K_{p1}})\Delta x_1 s + \frac{1}{K_{p1}}\Delta x_1 + (T_{t1}T_r\Delta P_{L1} + T_{t1}T_r\Delta P_{tie1})s^2 \tag{4.23}$$

$$+ (T_{t1}\Delta P_{L1} + T_{t1}\Delta P_{tie1} + T_r\Delta P_{L1} + T_r\Delta P_{tie1})s + (\Delta P_{L1} + \Delta P_{tie1})\}$$

From (3.9), the relationship between control signal and the valve/gate position change is developed as

$$\left(u_1 - \frac{1}{R_1}\Delta x_1\right).\frac{1}{1+T_{g1}s} = \Delta X_{g1} \tag{4.24}$$

Substituting (4.23) into (4.24) yields

$$\Delta x_1 s^4 = \alpha_1\Delta x_1 s^3 + \alpha_2\Delta x_1 s^2 + \alpha_3\Delta x_1 s + \alpha_4\Delta x_1 - \frac{K_{p1}}{T_{p1}}(\Delta P_{L1} + \Delta P_{tie1})s^3$$

$$+ \alpha_5(\Delta P_{L1} + \Delta P_{tie1})s^2 + \alpha_6(\Delta P_{L1} + \Delta P_{tie1})s - \frac{K_{p1}}{T_{g1}T_{t1}T_rT_{p1}}(\Delta P_{L1} + \Delta P_{tie1})$$

$$+ \frac{K_{p1}}{T_{g1}T_{t1}T_rT_{p1}}(u_1 + K_rT_ru_1 s) \tag{4.25}$$

Where

$$\alpha_1 = -\left(\frac{1}{T_{g1}} + \frac{1}{T_{t1}} + \frac{1}{T_{p1}} + \frac{1}{T_r}\right) \tag{4.26}$$

$$\alpha_2 = -\left(\frac{1}{T_{g1}T_{t1}} + \frac{1}{T_{g1}T_{p1}} + \frac{1}{T_{g1}T_r} + \frac{1}{T_{t1}T_{p1}} + \frac{1}{T_{t1}T_r} + \frac{1}{T_rT_{p1}}\right) \tag{4.27}$$

$$\alpha_3 = -\frac{1}{T_{g1}T_{t1}T_rT_{p1}}(T_r + T_{t1} + T_{g1} + T_{p1} + \frac{K_{p1}K_rT_r}{R_1}) \tag{4.28}$$

$$\alpha_4 = -\frac{1}{T_{g1}T_{t1}T_rT_{p1}}(\frac{K_{p1}}{R_1} + 1) \tag{4.29}$$

$$\alpha_5 = -\left(\frac{K_{p1}}{T_{g1}T_{p1}} + \frac{K_{p1}}{T_{t1}T_{p1}} + \frac{K_{p1}}{T_rT_{p1}}\right) \tag{4.30}$$

$$\alpha_6 = -\frac{T_rK_{p1} + T_{t1}K_{p1} + T_{g1}K_{p1}}{T_{g1}T_{t1}T_rT_{p1}} \tag{4.31}$$

The ODE model of (4.25) is

$$\begin{aligned}\Delta x_1^{(4)} &= \alpha_1\Delta\dddot{x}_1 + \alpha_2\Delta\ddot{x}_1 + \alpha_3\Delta\dot{x}_1 + \alpha_4\Delta x_1 - \frac{K_{p1}}{T_{p1}}(\Delta\dddot{P}_{L1} + \Delta\dddot{P}_{tie1}) \\ &+ \alpha_5(\Delta\ddot{P}_{L1} + \Delta\ddot{P}_{tie1}) + \alpha_6(\Delta\dot{P}_{L1} + \Delta\dot{P}_{tie1}) - \frac{K_{p1}}{T_{g1}T_{t1}T_rT_{p1}}(\Delta P_{L1} + \Delta P_{tie1}) \\ &+ \frac{K_{p1}}{T_{g1}T_{t1}T_rT_{p1}}(u_1 + K_rT_r\dot{u}_1)\end{aligned} \tag{4.32}$$

Equation (4.32) shows a fourth-order ODE model for the frequency error in area 2. According to (4.2), we design the sliding surface as

$$s(\Delta x_1, t) = \left(\frac{d}{dt} + \delta\right)^3 \Delta \tilde{x}_1(t) = \Delta \dddot{\tilde{x}}_1(t) + 3\delta \Delta \ddot{\tilde{x}}_1(t) + 3\delta^2 \Delta \dot{\tilde{x}}_1(t) + \delta^3 \Delta \tilde{x}_1(t) \tag{4.33}$$

In (4.33), the desired frequency error is zero. So we have

$$\Delta \tilde{x}_1(t) = \Delta x_1(t) - \Delta x_d(t) = \Delta x_1(t) - 0 = \Delta x_1(t) \tag{4.34}$$

The derivative of the sliding surface is

$$\dot{s}(\Delta x_1, t) = \Delta x_1^{(4)}(t) + 3\delta \Delta \dddot{x}_1(t) + 3\delta^2 \Delta \ddot{x}_1(t) + \delta^3 \Delta \dot{x}_1(t) \tag{4.35}$$

We define the output of SMC as w, and

$$w = u_1 + K_r T_r \dot{u}_1 \tag{4.36}$$

Let the derivative of sliding surface be equal to zero. We will have the equivalent control law wˆ as

$$\begin{aligned} \hat{w} = -\frac{T_{g1} T_{t1} T_r T_p}{K_{p1}} [&\alpha_1 \Delta \dddot{x}_1 + \alpha_2 \Delta \ddot{x}_1 + \alpha_3 \Delta \dot{x}_1 + \alpha_4 \Delta x_1 - \frac{K_{p1}}{T_{p1}} (\Delta \dddot{P}_{L1} + \Delta \dddot{P}_{tie1}) \\ &+ \alpha_5 (\Delta \ddot{P}_{L1} + \Delta \ddot{P}_{tie1}) + \alpha_6 (\Delta \dot{P}_{L1} + \Delta \dot{P}_{tie1}) - \frac{K_{p1}}{T_{g1} T_{t1} T_r T_{p1}} (\Delta P_{L1} + \Delta P_{tie1}) \\ &+ 3\delta \Delta \dddot{x}_1(t) + 3\delta^2 \Delta \ddot{x}_1(t) + \delta^3 \Delta \dot{x}_1(t)] \end{aligned} \tag{4.37}$$

The control effort of w in area 1 is a nonlinear combination of equivalent control law and switch control law, which is a sign function. The control effort can be represented as (4.38), where k_1 is a positive controller gain.

$$w(t) = \hat{w}(t) - K_1 \operatorname{sgn}(s(\Delta x_1, t)) \tag{4.38}$$

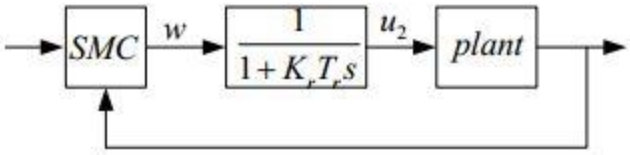

Figure 4.2 The Control System for the Power Control Area with Reheat Turbine

Figure 4.2 shows the control system for a power control area with reheat turbine. In this figure, plant is area 1.

4.2.2 SMC for the Area with Hydraulic Turbine

In this section, the SMC is applied to the power area with hydro turbine (area2 in Figure 3.14). We set the frequency error for the power system with hydro turbine as Δx_2.

$$\Delta f_2 = \Delta x_2 \tag{4.39}$$

From (3.30), the relationship between the frequency error and the mismatched power is derived as

$$\Delta P_{g2} = \Delta P_{L2} + \Delta P_{tie2} + \frac{T_{p2}}{K_{p2}}\Delta x_2 s + \frac{1}{K_{p2}}\Delta x_2 \tag{4.40}$$

From (3.17), we can obtain the relationship between the valve/gate position ΔX_{g2} and the mechanical power ΔP_{g2} in area 2. The relationship is given by

$$\Delta X_{g2} = \frac{1}{1-T_W s}\Delta P_{g2} + \frac{0.5T_W}{1-T_W s}\Delta P_{g2} s \tag{4.41}$$

Substituting (4.40) into (3.41), we get

$$\begin{aligned}\Delta X_{g2} &= \frac{1}{1-T_W s}(\Delta P_{L2} + \Delta P_{tie2} + \frac{T_{p2}}{K_{p2}}\Delta x_2 s + \frac{1}{K_{p2}}\Delta x_2) \\ &+ \frac{0.5T_W}{1-T_W s}(\Delta P_{L2} s + \Delta P_{tie2} + \frac{T_{p2}}{K_{p2}}\Delta x_2 s^2 + \frac{1}{K_{p2}}\Delta x_2 s)\end{aligned} \tag{4.42}$$

From (3.18), we can obtain the following equation, where ΔX_{gh} is an intermediate variable for area 2.

$$\frac{\Delta X_{g2}}{\Delta X_{gh}} = \frac{T_R s + 1}{T_2 s + 1} \tag{4.43}$$

Equation (4.43) can be rewritten as

$$\Delta X_{gh} = \frac{T_2}{T_R s + 1} \Delta X_{g2} s + \frac{1}{T_R s + 1} \Delta X_{g2} \tag{4.44}$$

Substituting (4.42) into (4.44) yields

$$\begin{aligned}
\Delta X_{gh} = {} & \frac{T_2}{T_R s + 1} [\frac{1}{1 - T_W s} (\Delta P_{L2} s + \Delta P_{tie2} s + \frac{T_{p2}}{K_{p2}} \Delta x_2 s^2 + \frac{1}{K_{p2}} \Delta x_2 s) \\
& + \frac{0.5 T_W}{1 - T_W s} (\Delta P_{L2} s^2 + \Delta P_{tie2} s + \frac{T_{p2}}{K_{p2}} \Delta x_2 s^3 + \frac{1}{K_{p2}} \Delta x_2 s^2) \\
& + \frac{1}{T_R s + 1} [\frac{1}{1 - T_W s} (\Delta P_{L2} + \Delta P_{tie2} + \frac{T_{p2}}{K_{p2}} \Delta x_2 s + \frac{1}{K_{p2}} \Delta x_2) \\
& + \frac{0.5 T_W}{1 - T_W s} (\Delta P_{L2} s + \Delta P_{tie2} + \frac{T_{p2}}{K_{p2}} \Delta x_2 s^2 + \frac{1}{K_{p2}} \Delta x_2 s)]
\end{aligned} \tag{4.45}$$

From (3.9), the relationship between control input u_2 and intermediate part ΔX_{gh} can be represented by

$$u_2 - \frac{1}{R_2} \Delta x_2 = T_{g2} \Delta X_{gh} s + \Delta X_{gh} \tag{4.46}$$

Substituting (4.45) into (4.46), we get

$$\begin{aligned}
\Delta x_2 s^4 = {} & -\gamma_1 \Delta x_2 s^3 - \gamma_2 \Delta x_2 s^2 - \gamma_3 \Delta x_2 s - \gamma_4 \Delta x_2 - \frac{K_{p2}}{T_{p2}} (\Delta P_{L2} + \Delta P_{tie2}) s^3 \\
& - \gamma_5 (\Delta P_{L2} + \Delta P_{tie2}) s^2 - \gamma_6 (\Delta P_{L2} + \Delta P_{tie2}) s \\
& - \frac{K_{p2}}{0.5 T_W T_2 T_{p2} T_{g2}} (\Delta P_{L2} + \Delta P_{tie2}) + \frac{T_R s + 1}{T_2 T_{g2}} \cdot \frac{1 - T_W s}{0.5 T_W} \cdot \frac{K_{p2}}{T_{p2}} u_2
\end{aligned} \tag{4.47}$$

Where

$$\gamma_1 = 1 + \frac{1}{T_{g2}} + \frac{1}{0.5T_W} + \frac{1}{T_2} \tag{4.48}$$

$$\gamma_2 = \frac{1}{0.5T_W T_{p2}} + \frac{1}{0.5T_W T_2} + \frac{1}{0.5T_W T_{g2}} + \frac{1}{T_{p2}T_{g2}} + \frac{1}{T_{p2}T_2} + \frac{1}{T_2 T_{g2}} - \frac{K_{p2}T_R T_W}{0.5T_W T_2 T_{g2} R_2 T_{p2}} \tag{4.49}$$

$$\gamma_3 = \frac{1}{0.5T_W T_{p2} T_2} + \frac{1}{0.5T_W T_{g2} T_{p2}} + \frac{1}{0.5T_W T_{g2} T_2} + \frac{1}{T_2 T_{p2} T_{g2}} + \frac{K_{p2}(T_R - T_W)}{0.5T_W T_2 T_{g2} R_2 T_{p2}} \tag{4.50}$$

$$\gamma_4 = \frac{R_2 + K_{p2}}{0.5T_W T_{g2} T_2 T_{p2} R_2} \tag{4.51}$$

$$\gamma_5 = \frac{K_{p2}}{0.5T_W T_{p2}} + \frac{K_{p2}}{T_{p2}T_2} + \frac{K_{p2}}{T_{p2}T_{g2}} \tag{4.52}$$

$$\gamma_6 = \frac{K_{p2}}{0.5T_W T_{p2} T_2} + \frac{K_{p2}}{0.5T_W T_{p2} T_{g2}} + \frac{K_{p2}}{T_2 T_{p2} T_{g2}} \tag{4.53}$$

The ODE model of (4.47) is

$$\begin{aligned} \Delta x_2^{(4)} = {} & -\gamma_1 \Delta \dddot{x}_2 R_2 - \gamma_2 \Delta \ddot{x}_2 - \gamma_3 \Delta \dot{x}_2 - \gamma_4 \Delta x_2 - \frac{K_{p2}}{T_{p2}} (\Delta \dddot{P}_{L2} + \Delta \dddot{P}_{tie2}) \\ & - \gamma_5 (\Delta \ddot{P}_{L2} + \Delta \ddot{P}_{tie2}) - \gamma_6 (\Delta \dot{P}_{L2} + \Delta \dot{P}_{tie2}) \\ & - \frac{K_{p2}}{0.5T_W T_2 T_{p2} T_{g2}} (\Delta P_{L2} + \Delta P_{tie2}) + \frac{-T_R T_W K_{p2} \ddot{u}_2 + K_{p2}(T_R - T_W)\dot{u}_2 + K_{p2} u_2}{0.5T_W T_2 T_{g2} T_{p2}} \end{aligned} \tag{4.54}$$

From (4.2), the sliding surface is designed as

$$s(\Delta x_2, u_2, w_2, t) = \left(\frac{d}{dt} + \delta\right)^3 \Delta \tilde{x}_2(t) = \Delta \dddot{\tilde{x}}_2(t) + 3\delta \Delta \ddot{\tilde{x}}_2(t) + 3\delta^2 \Delta \dot{\tilde{x}}_2(t) + \delta^3 \Delta \tilde{x}_2(t) \tag{4.55}$$

In (4.55), the desired frequency error is zero as shown in (3.56).

$$\Delta \tilde{x}_2(t) = \Delta x_2(t) - \Delta x_d(t) = \Delta x_2(t) - 0 = \Delta x_2(t) \tag{4.56}$$

The derivative of the sliding surface is

$$\dot{s}(\Delta x_2, t) = \Delta x_2^{(4)}(t) + 3\delta \Delta \dddot{x}_2(t) + 3\delta^2 \Delta \ddot{x}_2(t) + \delta^3 \Delta \dot{x}_2(t) \tag{4.57}$$

We define the output of SMC for area 2 as z and

$$z = -T_R T_W \ddot{u}_2 + (T_R - T_W)\dot{u}_2 + u \tag{4.58}$$

Let the derivative of the sliding surface be equal to zero. We will have equivalent control law z as

$$\hat{z} = \frac{0.5 T_W T_2 T_{g2} T_{p2}}{K_{p2}} [\gamma_1 \Delta \dddot{x}_2 R_2 + \gamma_2 \Delta \ddot{x}_2 + \gamma_3 \Delta \dot{x}_2 + \gamma_4 \Delta x_2 + \frac{K_{p2}}{T_{p2}} (\Delta \dddot{P}_{L2} + \Delta \dddot{P}_{tie2})$$

$$+ \gamma_5 (\Delta \ddot{P}_{L2} + \Delta \ddot{P}_{tie2}) + \gamma_6 (\Delta \dot{P}_{L2} + \Delta \dot{P}_{tie2}) \tag{4.59}$$

$$+ \frac{K_{p2}}{0.5 T_W T_2 T_{p2} T_{g2}} (\Delta P_{L2} + \Delta P_{tie2}) - 3\delta \Delta \dddot{x}_2(t) - 3\delta^2 \Delta \ddot{x}_2(t) - \delta^3 \Delta \dot{x}_2(t)$$

The real SMC control law for area 2 is a linear combination of equivalent control law and switch control law. It can be represented as (4.60), where k_2 is a positive controller gain.

$$z(t) = \hat{z}(t) - k_2 \operatorname{sgn}(s(\Delta x_2, t)) \tag{4.60}$$

Equation (4.58) shows the relationship between z and u_2 . From (4.47), we can see that the hydro turbine contains a positive zero ($s = 1/T_W$) We can compensate the effect of positive zero by adding a compensation function 1/-(s+a) where a is ranging from 0 to 50. Here we choose a as 50 based on simulation results. The overshoot percentage for frequency error is smaller as a=50 compared to the ones for other values of a. However, when we choose a as a value larger than 50, the overshoot percentage for frequency error will not decrease any more.

Figure 4.3 shows the control model for the power system with hydro turbine. In this figure, plant is area 2, and u'_2 is the output of compensation function.

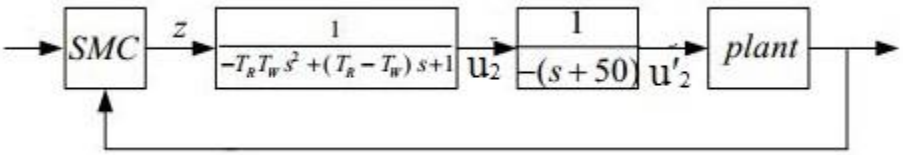

Figure 4.3 The Control System for the Power Control Area with Hydro Turbine

Chapter 5
SIMULATION RESULTS

In this chapter, VSC-FSMC is applied to single-area, two-area interconnected power systems respectively. The nonlinearities such as governor dead band (GDB) and the GRCs for turbines are included into the power system model in simulation. The effectiveness of proposed control method fuzzy sliding mode control (FSMC) is validated through the simulation results. In this design, variable structure concept (VSC) operation of sliding mode control (SMC) concept is applied in fuzzy logic controllers to demonstrate the performance of an interconnected hydro-thermal power plant load frequency control compare with other conventional interconnected hydro-thermal PI and hybrid neuro fuzzy controller using MATLAB/SIMULINK software. Figure 5.1, 5.2, 5.5 shows thermal-hydro model of variable structure concept operation of sliding mode control fuzzy logic controller. Figure 5.3-5.10, 5.11 – 5.14, 5.15 – 5.18 shows the simulation results graphical plot of thermal-Hydro model of VSC-SMC logic controller, thermal-Hydro PI controller and thermal-Hydro model of HNF logic controller respectively and figure 5.4, 5.9 shows the tie line power deviation response of thermal-Hydro model of VSC-FSMC logic controller. The responses shows that thermal-hydro combined plant with VSC-FSMC controller has better steady state error, settling time and % of overshoot compare to other combined controller. In single area system VSC-FSMC controller have the better dynamics compare to others.

5.1 Simulation Results for (VSC-FSMC) Single Area Power System with Reheat Thermal Turbine and Hydro Turbine

In this section, we simulate the FSMC method on the single area power system with reheat thermal and hydro turbine as shown in Figure 5.1 and Figure 5.2 respectively.

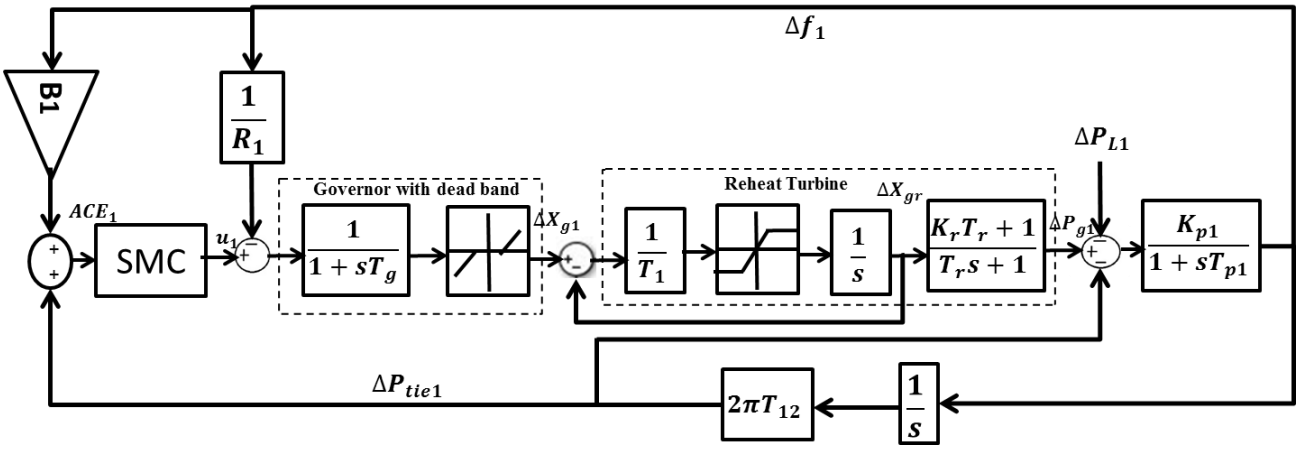

Figure 5.1 Single Area Power System with Reheat Thermal Turbine

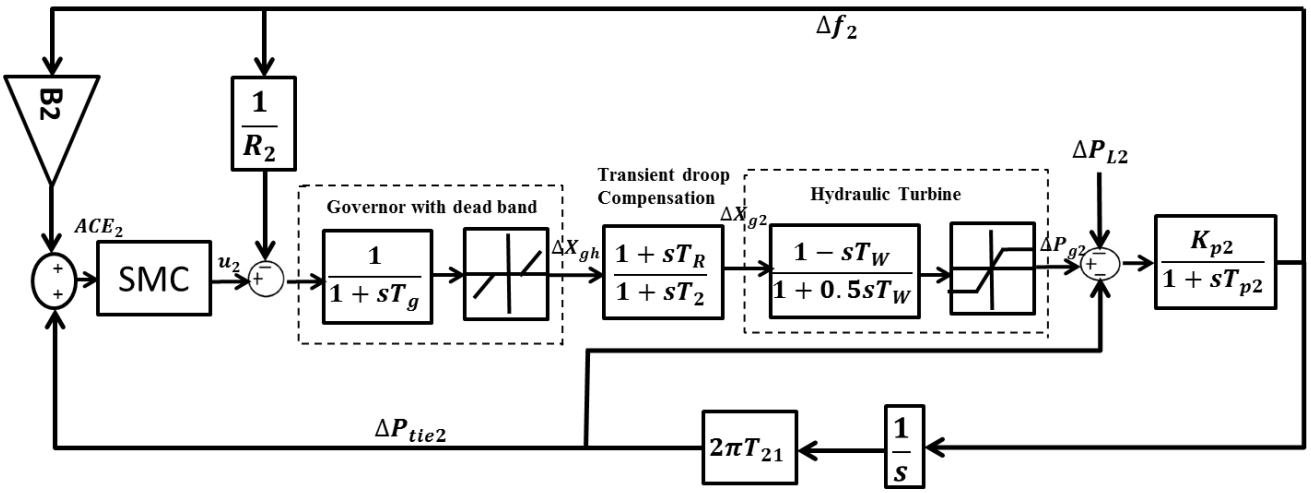

Figure 5.2 Single Area Power System with Hydro Turbine

In this section, we simulate the VSC-FSMC into single-area power systems with reheat and hydro turbines respectively. The simulation results are shown as follows. First, we simulate VSC-FSMC on the single area power system with a reheat turbine and hydro turbine. Figure 5.3 shows the single area power system frequency deviation and Figure 5.4 shows the single area power system tie line power deviation with reheat thermal and hydro turbine.

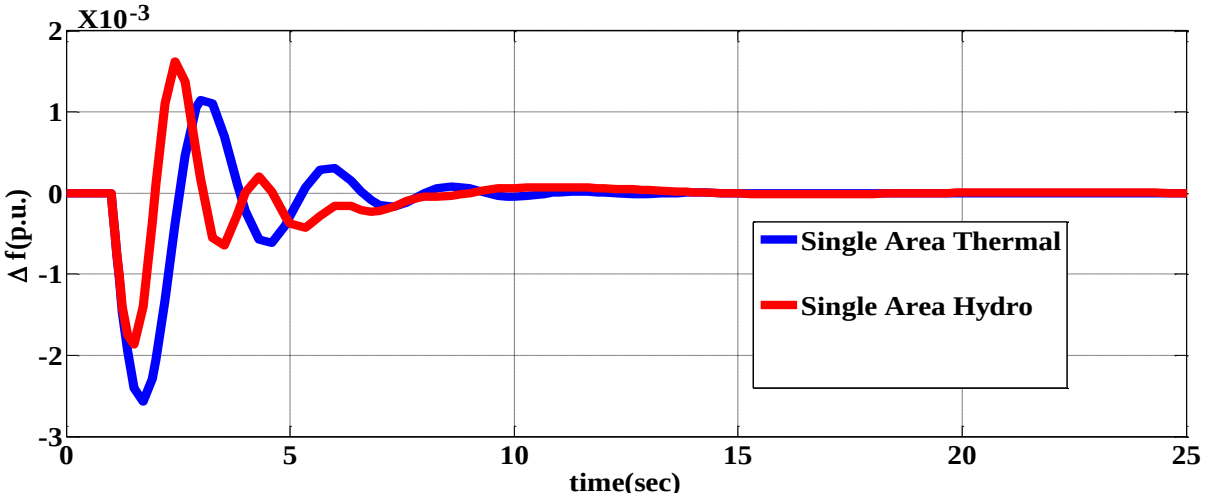

Figure 5.3 Single Area Power System frequency deviation with reheat Thermal and Hydro Turbine

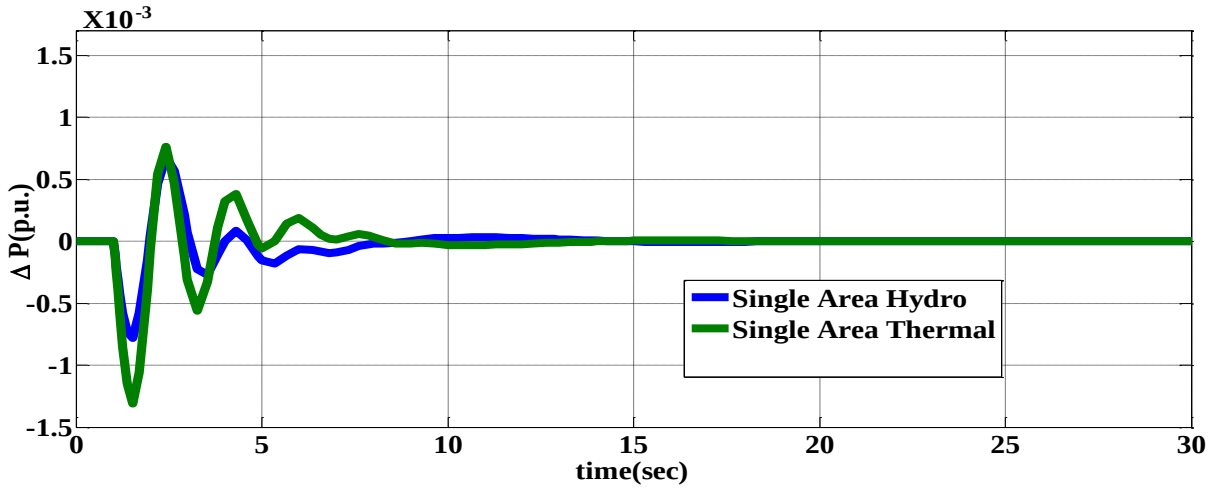

Figure 5.4 Single area power system tie line power deviation with reheat thermal and hydro Turbine

5.1.1 Simulation Results for (VSC-FSMC) the Two Area Interconnected Power System with Reheat Thermal Turbine and Hydro Turbine

Figure 5.5 shows a two-area interconnected power system with non-reheat turbines only. GDB and GRC are considered in the system as shown in Figure 5.5. The parameter values for the two area power system are listed in Appendix.

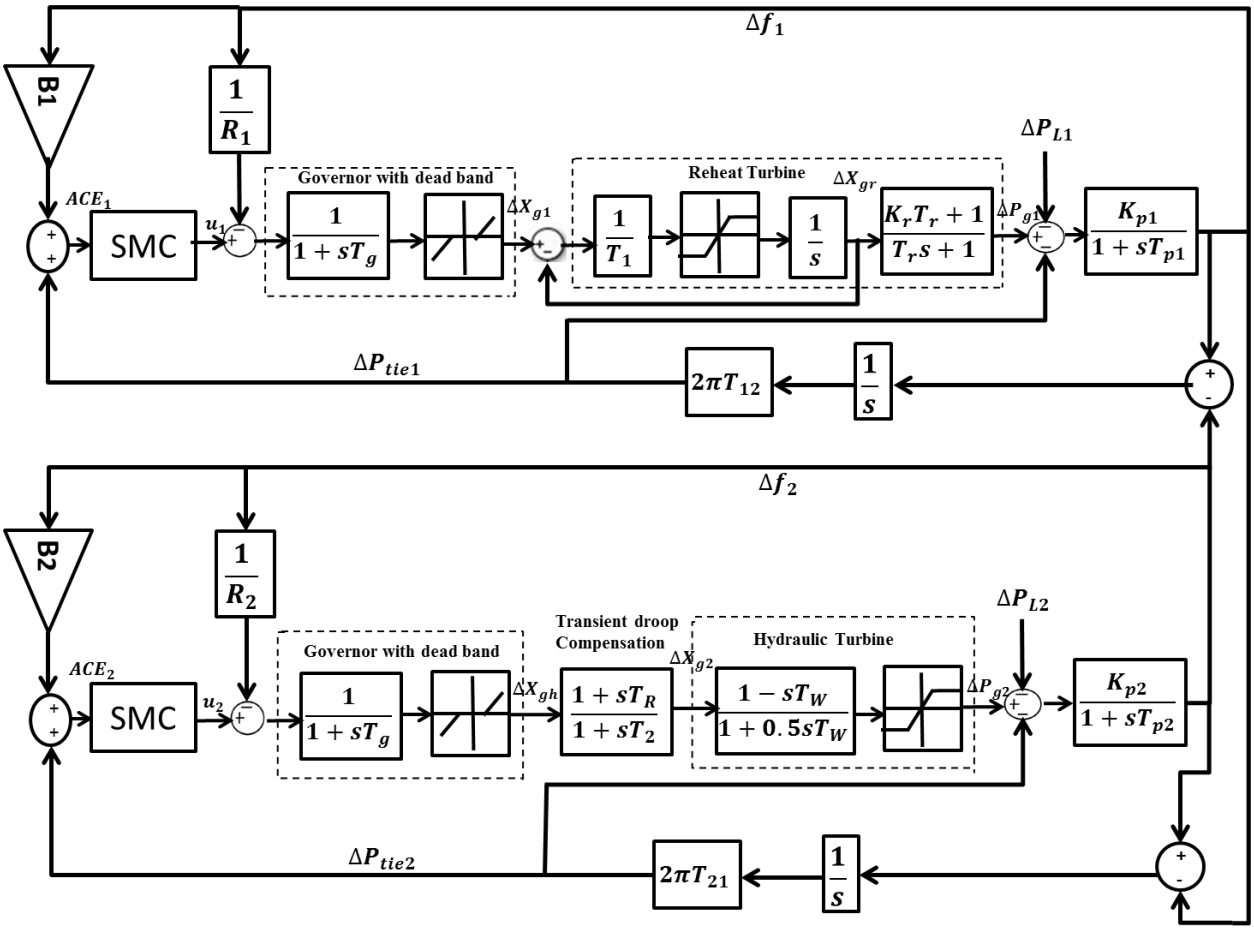

Figure 5.5 Two area power system of Thermal-Hydro plant of VSC-SMC fuzzy logic controller

In this part, we simulate the FSMC on two kinds of two-area interconnected power systems. In this part, we will show the simulation results for the two area interconnected power system. One area includes reheat turbine and the other area contains hydro turbine. Figure 5.6 shows the two area interconnected power system frequency deviation, Figure 5.7 shows the two area hydro-thermal interconnected power system frequency deviation, figure 5.9 shows the two area hydro-thermal interconnected power system tie line power deviation. Figure 5.8 and 5.10 shows the combination results of single and combined plant frequency deviation and tie line power deviation respectively.

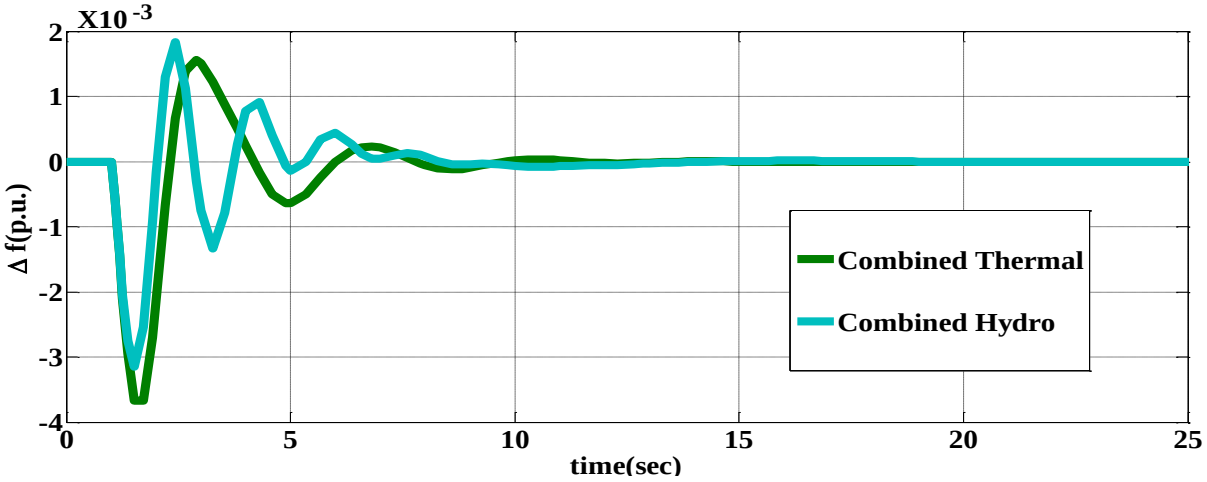

Figure 5.6 Two area interconnected power system frequency deviation with reheat thermal and hydro Turbine

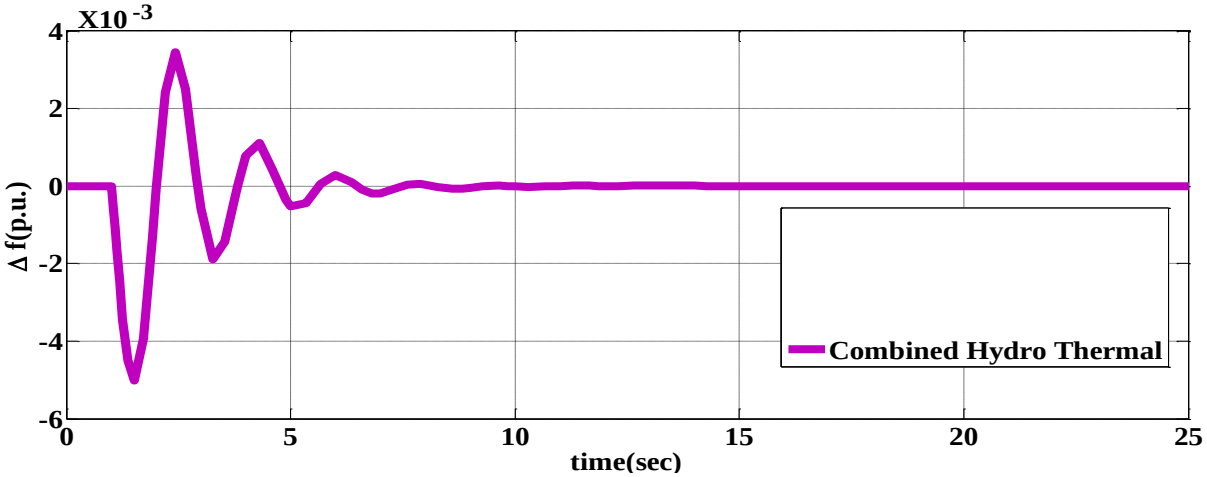

Figure 5.7 Two area interconnected power system frequency deviation with reheat thermal and hydro Turbine

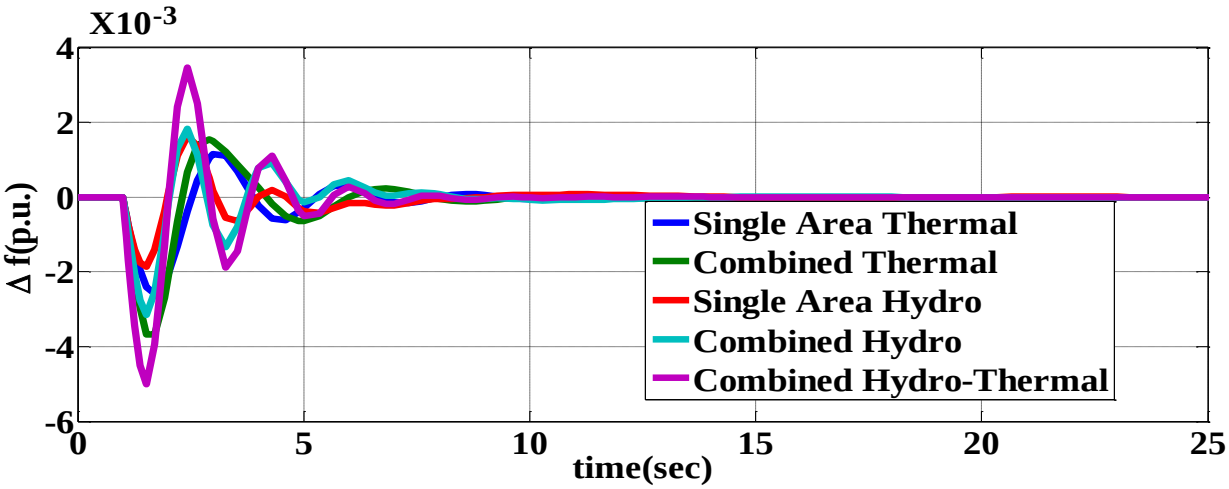

Figure 5.8 VSC-FSMC controller response of thermal-hydro plant

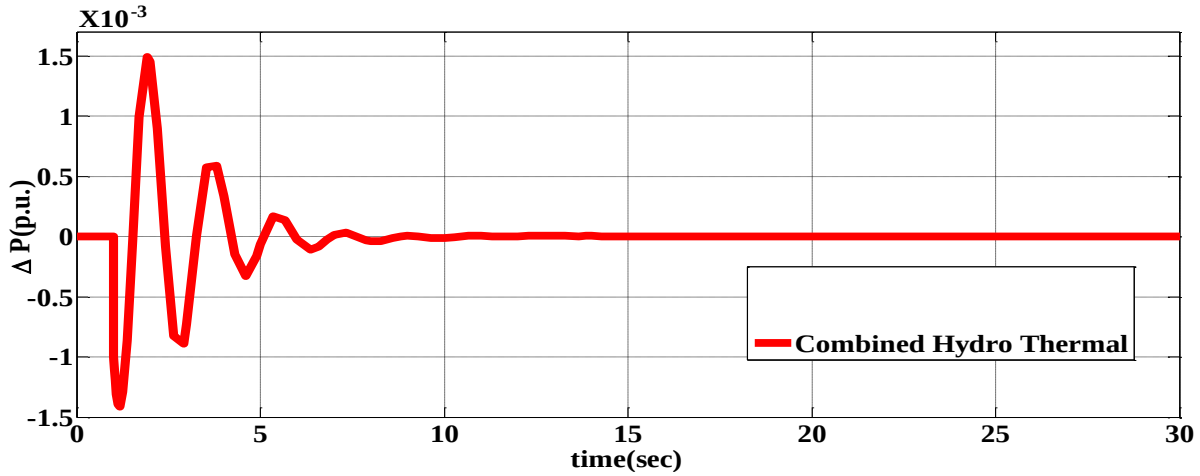

Figure 5.9 Two area interconnected power system tie line power deviation with reheat thermal and hydro Turbine

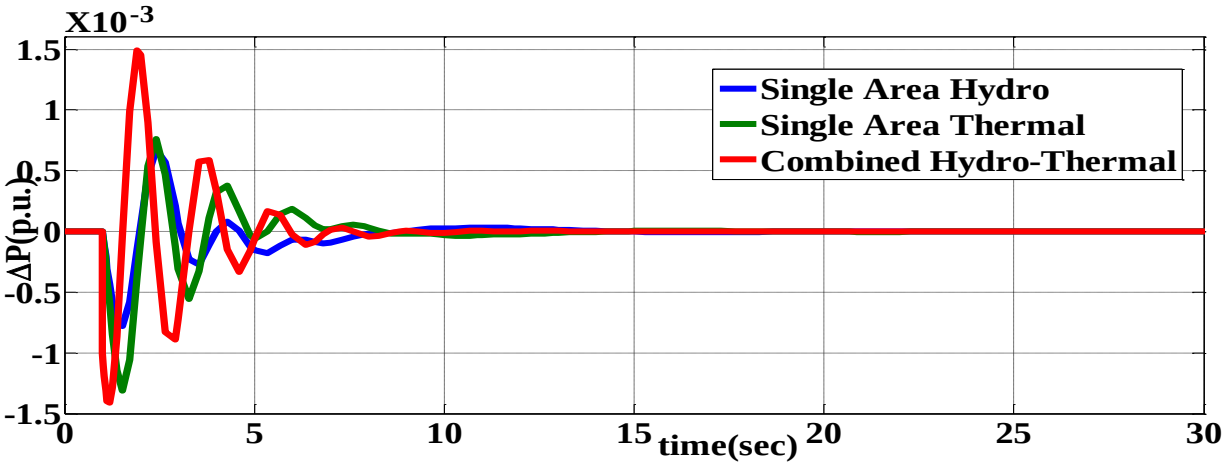

Figure 5.10 VSC-FSMC controller response of thermal-hydro plant

5.2 Simulation Results Using PI Controller for Single Area Power System with Reheat Thermal Turbine and Hydro Turbine

In this section, we simulate the PI controller onto single-area power systems with reheat and hydro turbines respectively. The simulation results are shown as follows. First, we simulate PI on the single area power system with a reheat turbine and hydro turbine. Figure 5.11 shows the single area power system frequency deviation.

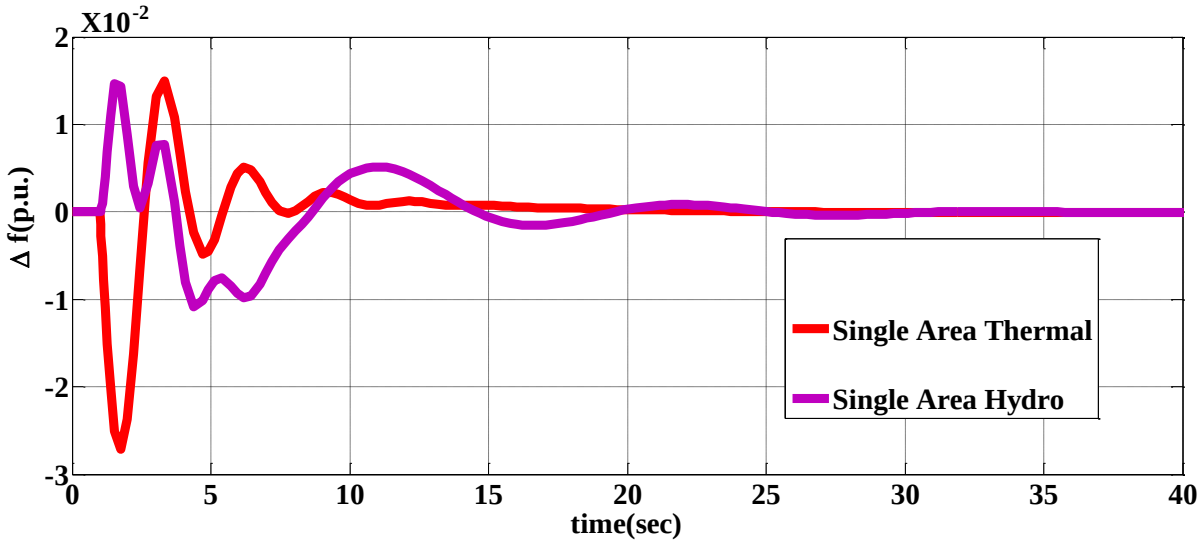

Figure 5.11 Single Area Power System frequency deviation with reheat Thermal and Hydro Turbine using PI controller

5.2.1 Simulation Results Using PI Controller for the Two Area Interconnected Power System with Reheat Thermal Turbine and Hydro Turbine

In this part, we simulate the PI on two kinds of two-area interconnected power systems. In this part, we will show the simulation results for the two area interconnected power system. One area includes reheat turbine and the other area contains hydro turbine. Figure 5.12 shows the two area interconnected power system frequency deviation, Figure 5.13 shows the two area hydro-thermal interconnected power system frequency deviation and 5.14 shows the combination results of single and combined plant frequency deviation.

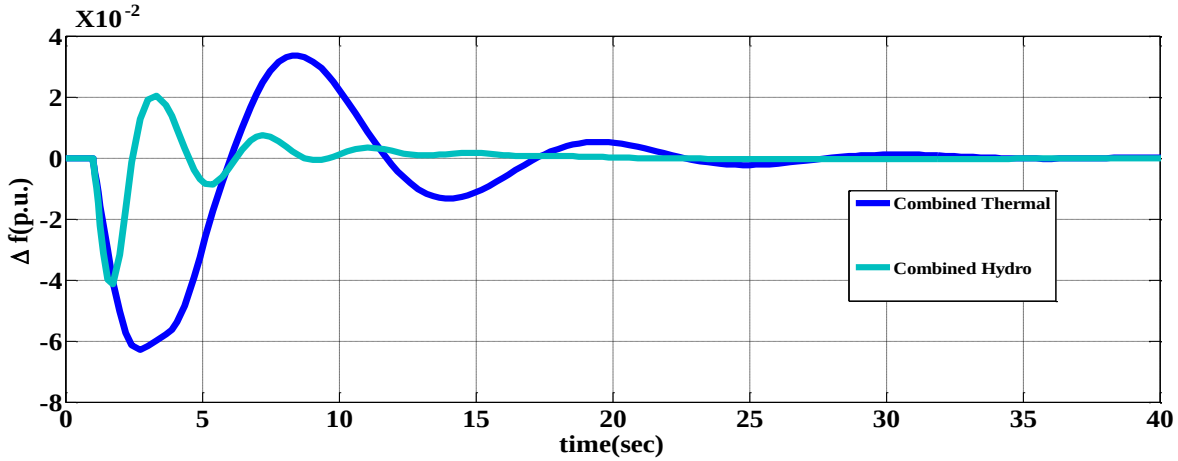

Figure 5.12 Two Area Power System frequency deviation with reheat Thermal-Thermal and Hydro-Thermal Turbine using PI controller

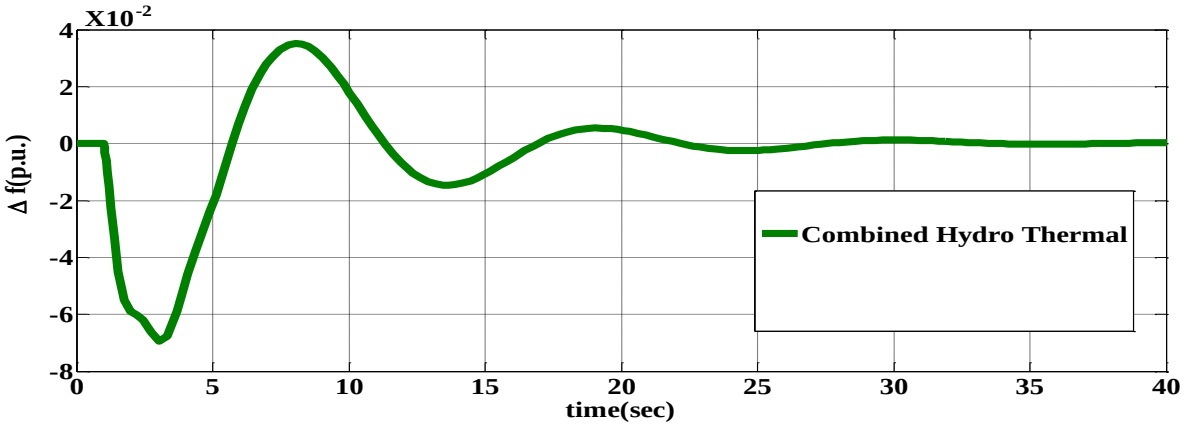

Figure 5.13 Two Area Power System frequency deviation with reheat Hydro -Thermal Turbine using PI controller

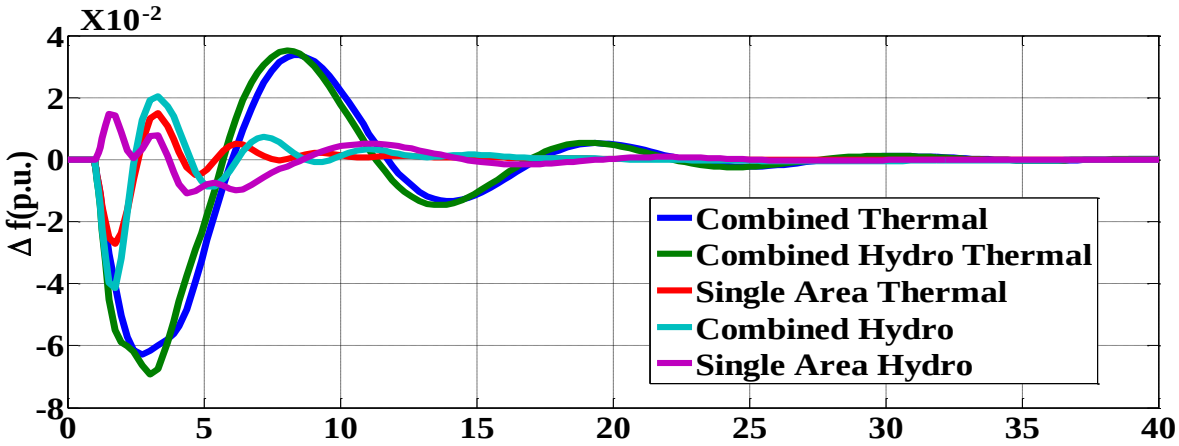

Figure 5.14 PI controller response of Hydro -Thermal plant

5.3 Simulation Results Using Hybrid Neuro Fuzzy Controller for Single Area Power System with Reheat Thermal Turbine and Hydro Turbine

In this section, we simulate the HNF controller onto single-area power systems with reheat and hydro turbines respectively. The simulation results are shown as follows. First, we simulate HNF on the single area power system with a reheat turbine and hydro turbine. Figure 5.15 shows the single area power system frequency deviation.

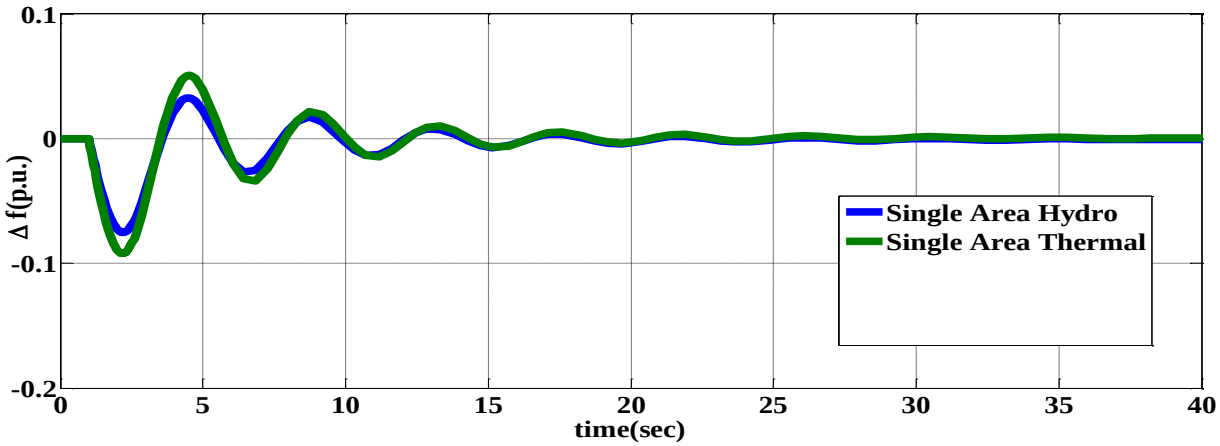

Figure 5.15 Single Area Power System frequency deviation with reheat Thermal and Hydro Turbine using Hybrid Neuro Fuzzy controller

5.3.1 Simulation Results Using Hybrid Neuro Fuzzy Controller for the Two Area Interconnected Power System with Reheat Thermal Turbine and Hydro Turbine

In this part, we simulate the HNF on two kinds of two-area interconnected power systems. In this part, we will show the simulation results for the two area interconnected power system. One area includes reheat turbine and the other area contains hydro turbine. Figure 5.16 shows the two area interconnected power system frequency deviation, Figure 5.17 shows the two area hydro-thermal interconnected power system frequency deviation and 5.18 shows the combination results of single and combined plant frequency deviation.

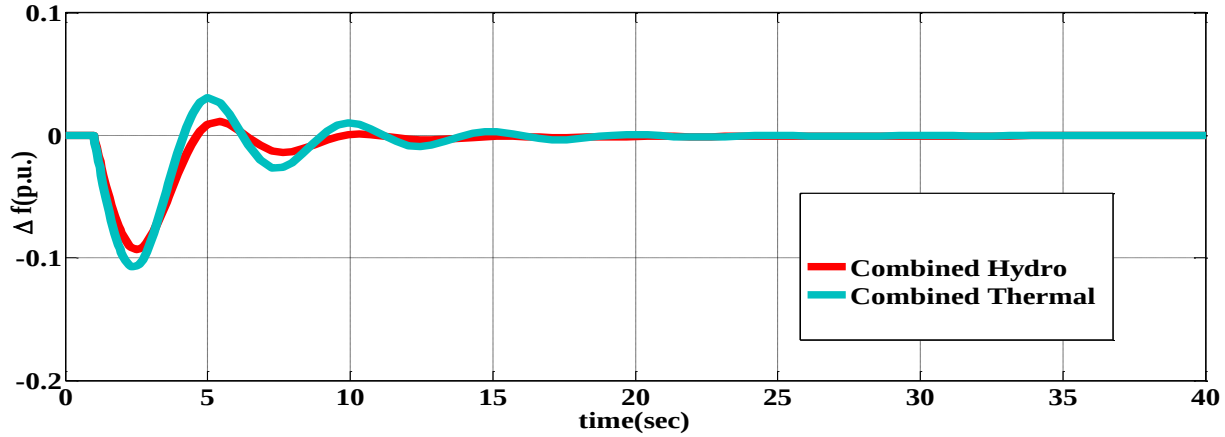

Figure 5.16 Two Area Power System frequency deviation with reheat Thermal- Thermal and Hydro-Hydro Turbine using Hybrid Neuro Fuzzy controller

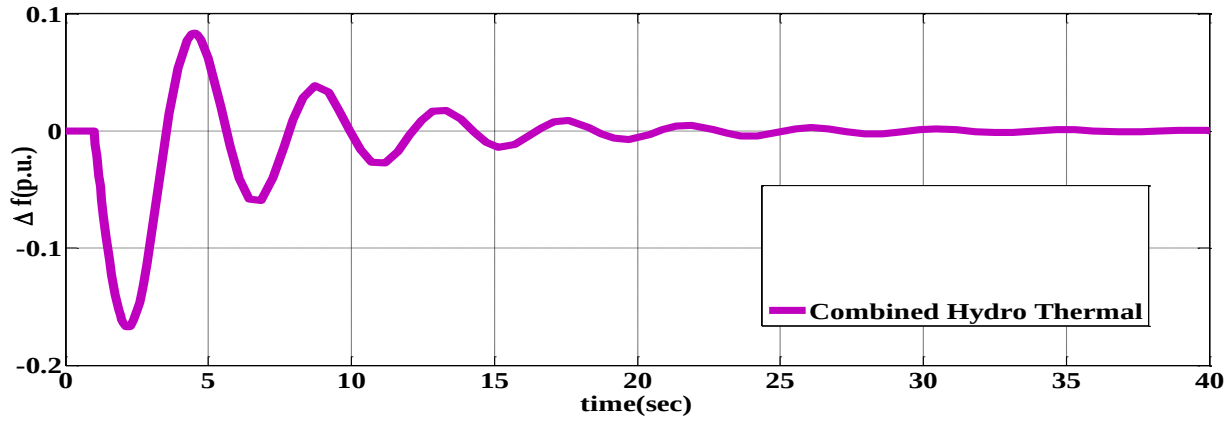

Figure 5.17 Two Area Power System frequency deviation with reheat Hydro -Thermal Turbine using Hybrid Neuro Fuzzy controller

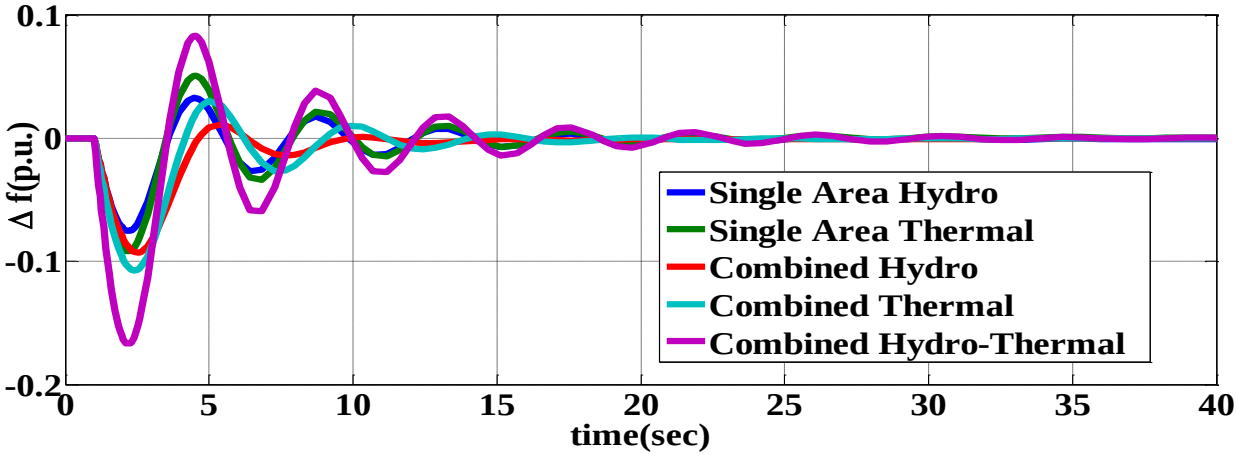

Figure 5.18 HNF controller response of thermal-hydro plant

5.4 Simulation Results Comparing VSC-FSMC with PI And HNF for the Two Area Interconnected Power System

Finally, we compare the proposed FSMC method with proportional integral and hybrid neuro fuzzy control method. Here, we choose proportional integral and hybrid neuro fuzzy control method because it is a dominant control method in industry for the load frequency control. The comparative results of the controller's outputs are shown in the Table 5.1.

TABLE 5.1 COMPARATIVE RESULTS OF CONTROLLERS OUTPUTS

Case of Simulation (1% load variation)	Steady State Error	Settling Time (Sec)	%of Overshoot
Thermal-hydro combined plant with VSC-FSMC controller (Δf)	0.000267	24.65739	0.999396
Thermal single area plant with VSC-FSMC controller(Δf)	0.000126	16.85582	0.99989
Hydro single area plant with VSC-FSMC controller(Δf)	-0.00091	24.6574	0.999415
Thermal-hydro combined plant with VSC-FSMC controller(ΔP)	0.0002795	25.657399	0.999457
Thermal single area plant with VSC-FSMC controller(ΔP)	0.0001747	22.289296	0.999684
Hydro single area plant with VSC-FSMC controller(ΔP)	$-6.68x10^{-5}$	21.289293	0.999785
Thermal-hydro combined plant with HNF controller(Δf)	0.0012	35.94542	0.983291
Thermal single area plant with HNF controller (Δf)	-0.00097	23.1503	0.914728
Hydro single area plant with HNF controller (Δf)	-0.00023	25.53542	0.992537
Thermal-hydro combined plant with PI controller (Δf)	0.00115	45.27102	0.999809
Thermal single area plant with PI controller (Δf)	-0.00269	27.06695	0.998207
Hydro single area plant with PI controller (Δf)	0.00958	37.83546	0.99529

1% step load increases is applied in this system to check the controller performance. The time required to stay 2% to 5% of any response final value that is the settling time of this response. In this case it is confirm that settling time is consider for 0.01% of final value and it shows the robustness and stability of

the controller. The designed controller has the minimum settling time compare to others controller 24.66 seconds and 25.65 seconds for combined hydro-thermal plant frequency and tie line power deviation respectively.

After the transient response steady state response is found and steady state error shows the accuracy of the controller. From figures 5.3 – 5.10 show the steady state errors of combined and single area are very close to zero which confirms the better dynamic performance of the VSC-FSMC controller.

At the peak time the amount that the wave form overshoots the steady-state or final value is expressed as a percentage of the steady state value that the Percent of overshoot. Percentage overshoot is the maximum value of a response minus final value divided by final value of the response. Compare to all of figures 5.3-5.18 result shows percent overshoots are better for designed controller.

Chapter 6

CONCLUSIONS AND FUTURE RESEARCH

In this dissertation, VSC-FSMC is applied in two area interconnected power system with two different kinds of turbines. The FSMC is originally simulated on the two-area interconnected power system with nonlinearities. The FSMC is tested on one-area and two-area power systems. The simulation results show that frequency deviation and tie-line power deviation are driven to zero successfully under different load disturbances. The simulation results verified the robustness of the control method against load disturbance. In addition, the system responses for variable structure based sliding mode based LFC are compared with the ones for a conventional proportional integral control based LFC and hybrid neuro fuzzy. The simulation results show the superiority of the variable structure based sliding mode based LFC to proportional integral control based LFC and hybrid neuro fuzzy controller in terms of steady state error, settling time and overshoot percentage. Theoretically the ideal sliding mode implies infinite switching frequency. Oscillations having finite frequency, which is known as 'chattering'. Chattering is a harmful phenomenon because it leads to low control accuracy, high wear of moving mechanical parts, and high heat losses in electrical power circuits. Since the control is constant within a sampling interval, switching frequency cannot exceed that of sampling, which leads to chattering as well. In the future, the FSMC based LFC will be improve by reducing the chattering effect.

In this work dynamic analysis of variable structure based sliding mode intelligent load frequency control of interconnected nonlinear conventional and renewable power system has been carried out using advanced fuzzy logic controller. A new model using variable structure concept of sliding mode fuzzy logic controller has been proposed and compared with the conventional PI and HNF controller with some step load variation in power system. The model is simple and gives better dynamics of settling time, steady state error and % of overshoot and reduces the oscillation of the frequency deviation compared to conventional models.

Simulation results show that the designed VSC-FSMC is more effective for improving the dynamic performance and stability of the interconnected power system compared to the conventional controller. When the VSC-FSMC is considered the proposed controller ensures the stability of power areas for any load demand variations and still achieves good dynamic performance for both single area and interconnected two area system. The proposed controller model is effective and provides significant improvement in the power system performance.

REFERENCES

[1] Reza Farhangi, Mehrdad Boroushaki, Seyed Hamid Hosseini, "Load frequency control of interconnected power system using emotional learning-based intelligent controller," Elsevier, Electrical Power and Energy Systems 36, 76–83, December 2011.

[2] Muthana T. Alrifai, Mohamed F. Hassan, "Load frequency controller for a multi-area interconnected power system", Elsevier, Electrical Power and Energy Systems 33, 198–209, August 2010.

[3] L. Dong, Y. Zhang, and Z. Gao, "A robust decentralized load frequency controller for interconnected power systems," International Society of Automation (ISA) Trans., vol. 51, pp. 410–419, 2012.

[4] Dola Gobinda Padhan and Somanath Majhi ,"A new control scheme for PI load frequency controller of single-area and multi-area power systems", International Society of Automation (ISA) Transactions 52, 242–251, 2013.

[5] Khodabakh shian A, Hooshmand R. "A new PID controller design for automatic generation control of hydro power systems," International Journal of Electric Power Energy System;32(5):375–82, 2010.

[6] W. Tan and Z. Xu, "Robust analysis and design of load frequency controller for power systems," Elect. Power Syst. Res., vol. 79, no. 5, pp. 846–853, 2009.

[7] S.P Ghoshal and S. K. Goswami, "Application of GA based optimal integral gains in fuzzy based active power frequency control of non-reheat and reheat thermal generating systems", Electric Power Systems Research (EPSR) 67, 2003.

[8] Rerkpreedapong D, Hasanovic A, Feliachi A. "Robust load frequency controlusing genetic algorithms and linear matrix inequalities," IEEE Trans Power Syst;18(2):855–6, 2003.

[9] Gayadhar Panda, Sidhartha Panda and Cemal Ardil, "Automatic Generation Control of Interconnected Power System by Hybrid Neuro Fuzzy Approach", World Academy of Science, Engineering and Technology International Journal of Electrical, Computer, Electronics and Communication Engineering Vol:6 No:4, 2012.

[10] Hassan A. Yousef, Khalfan Mohammed Al Kharusi, "Indirect Adaptive Fuzzy Logic frequency control of Multi-area Power System", Proceedings of the 8th IEEE GCC Conference and Exhibition, Muscat, Oman, 1-4 February, 2015.

[11] H. A. Yousef, K. AL-Kharusi, M. Albadi, and N. Hosseinzadeh, " Load Frequency Control of a Multi-Area Power System: An Adaptive Fuzzy Logic Approach", IEEE Trans. On Power Systems, VOL. 29, NO, pp.1822-1830, 2014.

[12] C. Srinivasa Rao, S. Siva Nagaraju, P. Sangameswara Raju, "Automatic generation control of TCPS based hydrothermal system under open market scenario: A fuzzy logic approach", Elsevier, Electrical Power and Energy Systems 31, 315–322, 2013.

[13] S. H. Hosseini and A. H. Etemadi, "Adaptive neuro-fuzzy inference system based automatic generation control," Electronic Power Syst. Res, vol. 78, pp. 1230–1239, 2008.

[14] Anand, B. And Ebenezer, A.J., "Load Frequency control with fuzzy logic controller considering Nonlinearities and Boiler Dynamic", The International Congress for global Science and Technology ICGST International Journal on Automatic Control & System Engineering (ACSE) , ICGST-ACSE Journal vol. 8, issue 111, 2009.

[15] H. Golpira and H. Bevrani, "Application of GA optimization for automaticgeneration control in realistic interconnected power system," in Proceedings ofInternational Conference on Modeling, Identification and Control, Okayama,Japan, July 17-19, 2010.

[16] R. Francis and I. A. Chidambaram, "Control performance standard based load frequency control of a two area reheat interconnected power system considering governor dead band nonlinearity using fuzzy neural network," International Journal of Computer Applications, vol. 46, no. 15, pp. 41-48, May, 2012.

[17] J. P. Lee and H. G. Kim, "Application of FESS controller for load frequency control," Journal of International Conference on Electric Machines and System, vol. 2, no. 3, pp. 361-366, 2013.

[18] A. M. Yousef, J. A. Khamaj and A. S. Oshaba, "Steam hydraulic turbines load frequency controller based on fuzzy logic control," Research Journal of Applied Sciences, Engineering and Technology, vol. 4, no. 15, pp. 2375-2381, 2012.

[19] H. Golpira and H. Bevrani, "Effect of physical constraints on the AGC dynamic behavior in an interconnected power system," International Journal of Advanced Mechatronic Systems, vol. 3, no. 2, pp. 79-87, 2011.

[20] M. A. Hanley, "Frequency Instabilities in North America Interconnections," National Energy Technology Laboratory, Tech. Report. May, 2011.

[21] "Frequency Response Initiative Report," North American Electric Corporation, Atlanta, GA, Tech. Report. October, 2012.

[22] S. R. Khuntia and S. Panda, "Simulation study for automatic generation control of a multi-area power system by ANFIS approach." Applied Soft Computing, vol. 12, no. 1, pp. 333-341, 2012.

[23] H. Bevrani and P. R. Daneshmand, "Fuzzy logic-based load-frequency control concerning high penetration of wind turbines," IEEE System Journal, vol. 6, no. 1, pp. 173-180, 2012.

[24] T. H. Mohamed, H. Bevrani, A. A. Hassan and T. Hiyama, "Decentralized model predictive based load frequency control in an interconnected power system," Energy Conversion and Management, vol. 52, no. 2, pp. 1208-1214, February 2011.

[25] R. Francis and I. A. Chidambaram, "Control performance standard based load frequency control of a two area reheat interconnected power system considering governor dead band nonlinearity using fuzzy neural network," International Journal of Computer Applications, vol. 46, no. 15, pp. 41-48, May, 2012.

[26] R. Farhangi, M. Boroushaki and S. H. Hosseini, "Load-frequency control of interconnected power system using emotional-learning based intelligent controller," International Journal of Electrical Power & Energy System, vol. 36, no. 1, pp. 76-83, 2012.

[27] L. Dong, Y. Zhang and Z. Gao, "A robust decentralized load frequency controller for interconnected power system," ISA Transactions, vol. 51, no. 3, pp. 410-419, 2012.

[28] M. Yang, Y. Fu, C. Wang and P. Wang, "Decentralized sliding mode load frequency control for multi-area power system," IEEE Transactions on Power System, vol. 28, no. 4, pp. 4301-4309, 2013.

[29] J. Wang and X. Wang, "Advanced Sliding Mode Control for Mechanical System," Beijing, China, Tsinghua University Press, 2012.

[30] Y. Zhao, "Applications of sliding mode controller and linear active disturbance rejection controller to a PMSM speed system," Department of Electrical and Computer Engineering, Cleveland State University, Cleveland, OH, USA, 2013.